

MULTI-OBJECTIVE PERFORMANCE BASED DESIGN OPTIMIZATION  
OF STEEL STRUCTURES

A THESIS SUBMITTED TO  
THE GRADUATE SCHOOL OF NATURAL AND APPLIED SCIENCES  
OF  
MIDDLE EAST TECHNICAL UNIVERSITY

BY  
HASAN ESER

IN PARTIAL FULFILLMENT OF THE REQUIREMENTS  
FOR  
THE DEGREE OF DOCTOR OF PHILOSOPHY  
IN  
CIVIL ENGINEERING

MAY 2021



Approval of the thesis:

**MULTI-OBJECTIVE PERFORMANCE BASED DESIGN OPTIMIZATION  
OF STEEL STRUCTURES**

submitted by **HASAN ESER** in partial fulfillment of the requirements for the degree  
of **Doctor of Philosophy in Civil Engineering, Middle East Technical University**  
by,

Prof. Dr. Halil Kalıpçılar  
Dean, Graduate School of **Natural and Applied Sciences**

Prof. Dr. Ahmet Türer  
Head of the Department, **Civil Engineering**

Prof. Dr. Oğuzhan Hasaebi  
Supervisor, **Civil Engineering, METU**

Prof. Dr. Ahmet Yakut  
Co-Supervisor, **Civil Engineering, METU**

**Examining Committee Members:**

Prof. Dr. Murat Altuğ Erberik  
Civil Engineering, METU

Prof. Dr. Oğuzhan Hasaebi  
Civil Engineering, METU

Assoc. Prof. Dr. Saeid Kazemzadeh Azad  
Civil Engineering, Atılım University

Assoc. Prof. Dr. Baki Öztürk  
Civil Engineering, Hacettepe University

Asst. Prof. Dr. Bekir Özer Ay  
Architecture, METU

Date: 03.05.2021

**I hereby declare that all information in this document has been obtained and presented in accordance with academic rules and ethical conduct. I also declare that, as required by these rules and conduct, I have fully cited and referenced all material and results that are not original to this work.**

Name, Last name : Hasan Eser

Signature :

## **ABSTRACT**

### **MULTI-OBJECTIVE PERFORMANCE BASED DESIGN OPTIMIZATION OF STEEL STRUCTURES**

Eser, Hasan  
Doctor of Philosophy, Civil Engineering  
Supervisor : Prof. Dr. Oğuzhan Hasaebi  
Co-Supervisor: Prof. Dr. Ahmet Yakut

May 2021, 101 pages

Seismic performance of structures designed in accordance with conventional force-based design (FBD) codes can vary significantly since (1) estimation and distribution of earthquake loads are based on initial stiffness of members and (2) force reduction factors are based on the rough assumption that all members will yield simultaneously. In recent decades, attempts to predict the seismic performance of structures resulted in the development of several guidelines for evaluation and rehabilitation of existing buildings (e.g., FEMA 273/356, ASCE/SEI 41). On the contrary, currently there is no performance-based design (PBD) code. As a matter of fact, while seismic performance assessment of existing buildings is a difficult task alone due to wide range of variabilities involved in seismic design parameters; PBD of a new structure by conventional means is practically impossible as size and detailing of members are also unknown at the start of the design process, yielding in numerous alternative design solutions. Although it is possible to automate the PBD process by optimization methods, a large number of nonlinear analyses required during optimization process take excessive computational time.

In this study, a novel design-driven optimization technique called Capacity Controlled Search (CCS) is proposed for achieving time-efficient optimum design of steel structures under the FBD and PBD methodologies. The success of the proposed method is first numerically investigated and justified by comparing its performance with those of several metaheuristic techniques on FBD optimization problems featuring various 2-D and 3-D ordinary moment resisting steel frames. Later, the same steel frames are optimally designed by PBD approach using the CCS method. A comparison of optimally designed structures via FBD and PBD methodologies is then carried out in terms of design cost and seismic performance. Finally, a practical multi-objective optimization approach is adopted to form the trade-off relationship between design cost and seismic performance, and alternative performance-based design solutions are presented.

The numerical results indicate the computational efficiency of the proposed optimization technique and suggest that more economical designs with predictable seismic performance can be produced for steel frames by the PBD approach than the conventional FBD.

**Keywords:** Performance Based Design, Structural Optimization, Multi-objective Optimization, Steel Frame Structures

## ÖZ

### ÇELİK YAPILARIN ÇOK-AMAÇLI PERFORMANS TABANLI TASARIM OPTİMİZASYONU

Eser, Hasan  
Doktora, İnşaat Mühendisliği  
Tez Yöneticisi: Prof. Dr. Oğuzhan Hasaebi  
Ortak Tez Yöneticisi: Prof. Dr. Ahmet Yakut

Mayıs 2021, 101 sayfa

Geleneksel kuvvet tabanlı tasarım standartlarına göre tasarlanan yapıların deprem performansları büyük farklılıklar gösterebilir. Bunun sebebi, deprem yüklerinin hesabının ve dağılımının, yapı elemanlarının rijitliklerinin ilk değerlerine baėlı olması ve deprem yükü azaltma katsayılarının tüm yapı elemanlarının aynı anda akmaya başlayacakları varsayımına dayanmasıdır. Son yıllarda, yapıların deprem performansını tahmin etme arayışı, mevcut yapıların performansını değerlendirmeye ve bu yapıların güçlendirilmesine yönelik kılavuzların geliştirilmesine olanak sağlamıştır (FEMA 273/356, ASCE/SEI 41). Öte yandan, hali hazırda yeni yapılar için performans tabanlı tasarım standardı bulunmamaktadır. Bunun esas sebebi, mevcut binaların deprem performansının değerlendirilmesi deprem tasarım parametrelerindeki sayısız deėişkene baėlı olarak başlı başına zor bir iş iken, yeni bir yapının konvansiyonel yöntemlerle performans tabanlı tasarımının, tasarım başında tüm bu deėişkenlere ek olarak yapı elemanlarının boyutları ve detaylandırmaları da belli olmadığından, pratik olarak neredeyse imkânsız olmasıdır. Optimizasyon yöntemleriyle her ne kadar performans tabanlı tasarım süreci

otomatize edilebilse de optimizasyon süresince gereken doğrusal olmayan analiz yöntemleri hesaplama sürelerini oldukça uzatmaktadır.

Bu çalışmada CCS adında, tasarım odaklı, yenilikçi bir optimizasyon tekniği geliştirilmiş ve geliştirilen bu tekniğin performansı bazı üstsezgisel algoritmalarla kıyaslanmıştır. Daha sonra geliştirilen bu teknikle optimize edilen kuvvet tabanlı ve performans tabanlı yapı tasarımlarının maliyet ve deprem performansları yönünden bir karşılaştırılması sunulmuştur. Son olarak pratik bir çok-amaçlı optimizasyon yaklaşımı kullanılarak, bu yapıların tasarım maliyeti ve deprem performansı arasındaki takas eğrileri oluşturulmuş, alternatif performans tabanlı tasarım çözümleri sunulmuştur.

Sayısal sonuçlar, geliştirilen tekniğin hesaplama verimliliğini ortaya çıkarırken; çelik çerçeve yapıların performans tabanlı tasarım yaklaşımıyla -geleneksel kuvvet tabanlı tasarım yaklaşımına kıyasla- daha ekonomik ve öngörülebilir deprem performansına sahip bir şekilde tasarlanabileceğine işaret etmektedir.

**Anahtar Kelimeler:** Performans Tabanlı Tasarım, Yapısal Optimizasyon, Çok-amaçlı Optimizasyon, Çelik Çerçeve Yapılar



To My Family

## ACKNOWLEDGMENTS

I wish to express my deepest gratitude to my supervisor Prof. Dr. Oğuzhan Hasaebi for his guidance, advice, criticism, encouragements, and insight throughout all phases of this research. The completion of this study would not be possible without his endless support and mentorship.

I sincerely thank my co-supervisor Prof. Dr. Ahmet Yakut for his guidance and insight, especially in laying the groundwork of this research.

I would also like to thank Prof. Dr. Murat Altuğ Erberik, Assoc. Prof. Dr. Saeid Kazemzadeh Azad, Assoc. Prof. Dr. Baki Öztürk, and Asst. Prof. Dr. Bekir Özer Ay for their invaluable suggestions and comments.

Special thanks to my family, friends and colleagues for their never-ending support and understanding during the preparation of the thesis.

## TABLE OF CONTENTS

ABSTRACT.....	v
ÖZ.....	vii
ACKNOWLEDGMENTS .....	x
TABLE OF CONTENTS.....	xi
LIST OF TABLES .....	xiv
LIST OF FIGURES .....	xvi
LIST OF ABBREVIATIONS .....	xviii
CHAPTERS	
1 INTRODUCTION .....	1
1.1 Structural Optimization at a Glance.....	1
1.2 An Overview of Performance Based Design .....	6
1.3 PBDO of Steel Moment Frame Structures: A Critical Review of the State-of-the-Art .....	9
1.4 Aim and Scope of the Thesis .....	14
2 PROBLEM FORMULATION.....	17
2.1 Design Variables and Objective Function .....	17
2.2 Design Constraints of FBDO Problem .....	18
2.3 Design Constraints of PBDO Problem .....	21
2.4 Penalized Objective Function .....	23
3 CAPACITY CONTROLLED SEARCH TECHNIQUE .....	25
3.1 The Working Principle of CCS.....	25
3.2 CCS Algorithm .....	30

4	VERIFICATION OF THE CCS TECHNIQUE.....	35
4.1	Numerical Examples .....	35
4.1.1	Example 1: 28-member planar OMRSF .....	37
4.1.2	Example 2: 54-member planar OMRSF .....	42
4.1.3	Example 3: 160-member OMRSF .....	47
4.1.4	Example 4: 584-member OMRSF .....	52
4.2	Summary.....	59
5	PERFORMANCE BASED DESIGN OPTIMIZATION .....	61
5.1	Performance Based Design using SAP2000 OAPI .....	61
5.2	Numerical Examples .....	62
5.2.1	Example 1: 28-member planar OMRSF .....	63
5.2.2	Example 2: 54-member planar OMRSF .....	66
5.2.3	Example 3: 160-member OMRSF .....	70
5.3	Summary.....	75
6	MULTI-OBJECTIVE PERFORMANCE BASED DESIGN OPTIMIZATION	
	77	
6.1	A Practical Approach for MOPBDO.....	77
6.2	Numerical Examples .....	78
6.2.1	Example 1: 28-member planar OMRSF .....	79
6.2.2	Example 2: 54-member planar OMRSF .....	81
6.2.3	Example 3: 160-member OMRSF .....	84
6.3	Summary.....	85
7	CONCLUSION .....	87
7.1	Summary and Concluding Remarks .....	87

7.2	Recommendations for Future Research .....	89
	REFERENCES .....	91
	CURRICULUM VITAE.....	101

## LIST OF TABLES

### TABLES

Table 1.1 An overview of studies on PBDO of steel moment frames .....	10
Table 4.1 Algorithm parameters for ADS, EBB-BC, and CCS .....	36
Table 4.2 Design loads and seismic coefficients .....	37
Table 4.3 Optimization statistics for 28-member planar OMRSF .....	39
Table 4.4 Optimum design for 28-member planar OMRSF.....	40
Table 4.5 DCRs for 28-member planar OMRSF.....	41
Table 4.6 Inter-story drift constraints for 28-member planar OMRSF .....	41
Table 4.7 Optimization statistics for 54-member planar OMRSF .....	43
Table 4.8 Optimum designs for 54-member planar OMRSF .....	44
Table 4.9 DCRs for 54-member planar OMRSF.....	46
Table 4.10 Inter-story drift constraints for 54-member planar OMRSF .....	46
Table 4.11 Optimization statistics for 160-member OMRSF .....	49
Table 4.12 Optimum designs for 160-member OMRSF.....	50
Table 4.13 DCRs for 160-member OMRSF.....	51
Table 4.14 Inter-story drift constraints for 160-member OMRSF (x-dir.).....	51
Table 4.15 Inter-story drift constraints for 160-member OMRSF (y-dir.).....	51
Table 4.16 Optimization statistics for 584-member OMRSF .....	54
Table 4.17 Optimum designs for 584-member OMRSF.....	55
Table 4.18 DCRs for 584-member OMRSF.....	57
Table 4.19 Inter-story drift constraints for 584-member OMRSF (x-dir.).....	58
Table 4.20 Inter-story drift constraints for 584-member OMRSF (y-dir.).....	58
Table 5.1 Optimum PBD and FBD for Example 1 .....	64
Table 5.2 Comparison of optimum PBD and FBD for Example 1. ....	64
Table 5.3 Optimum PBD and FBD for Example 2 .....	67
Table 5.4 Comparison of optimum PBD and FBD for Example 2 .....	67
Table 5.5 Optimum PBD and FBD for Example 3 .....	70
Table 5.6 Comparison of optimum PBD and FBD for Example 3 .....	71

Table 6.1 PBD alternatives for Example 1 .....	81
Table 6.2 PBD alternatives for Example 2 .....	83
Table 6.3 PBD alternatives for Example 3 .....	86

## LIST OF FIGURES

### FIGURES

Figure 2.1. Geometric (constructability) constraints .....	21
Figure 3.1. Adaptive search neighborhood width .....	32
Figure 4.1. 28-member planar OMRSF and grouping of structural elements .....	37
Figure 4.2. Optimization histories for 28-member planar OMRSF .....	40
Figure 4.3. 54-member planar OMRSF and grouping of structural elements .....	42
Figure 4.4. Optimization histories for 54-member planar OMRSF .....	45
Figure 4.5. 160-member OMRSF, (a) 3D-view (b) plan view .....	47
Figure 4.6. Optimization histories for 160-member OMRSF .....	50
Figure 4.7. 584-member OMRSF, (a) 3D-view (b) plan view .....	53
Figure 4.8. Optimization histories for 584-member OMRSF .....	56
Figure 5.1. Hinge states (BSE-2N) for optimum PBD (top) and FBD (bottom) for Example 1 .....	65
Figure 5.2. Pushover capacity curves of optimum PBD and FBD for Example 1 ..	65
Figure 5.3. Optimization history for Example 1 (PBD) .....	66
Figure 5.4. Hinge states (BSE-2N) for optimum PBD (top) and FBD (bottom) for Example 2 (+x loading) .....	68
Figure 5.5. Hinge states (BSE-2N) for optimum PBD (top) and FBD (bottom) for Example 2 (-x loading) .....	68
Figure 5.6. Pushover capacity curves of optimum PBD and FBD for Example 2 ..	69
Figure 5.7. Optimization history for Example 2 (PBD) .....	69
Figure 5.8. Hinge states (BSE-2N) for optimum PBD (top) and FBD (bottom) for Example 3 (+x loading) .....	72
Figure 5.9. Hinge states (BSE-2N) for optimum PBD (top) and FBD (bottom) for Example 3 (+y loading) .....	73
Figure 5.10. Pushover capacity curves of optimum PBD and FBD for Example 3 ..	74
Figure 5.11. Optimization history for Example 3 (PBD) .....	74
Figure 6.1. Feasible design solutions for Example 1 .....	80



Figure 6.2. Non-dominated design solutions for Example 1 .....	80
Figure 6.3. Feasible design solutions for Example 2 .....	82
Figure 6.4. Non-dominated design solutions for Example 2 .....	82
Figure 6.5. Feasible design solutions for Example 3 .....	84
Figure 6.6. Non-dominated design solutions for Example 3 .....	85

## LIST OF ABBREVIATIONS

### ABBREVIATIONS

ACO	Ant Colony Optimization
ADS	Adaptive Dimensional Search
ASA	Adaptive Simulated Annealing
CMOFA	Chaotic Multi-objective Firefly Algorithm
CSS	Charged System Search
DEO	Dolphin Echolocation Optimization
EBB-BC	Exponential Big Bang – Big Crunch
ECBO	Enhanced Colliding Bodies Optimization
ESMO	Evolution Strategies for Multi-objective Optimization
FBDO	Force Based Design Optimization
FC-MOPSO	Fast Converging Multi-objective Particle Swarm Optimization
GA	Genetic Algorithm
HS	Harmony Search
IQPSO	Improved Quantum Particle Swarm Optimization
MFA	Modified Firefly Algorithm
MGSO	Multi-objective Group Search Optimizer
MOGA	Multi-objective Genetic Algorithm
MOHPSO	Multi-objective Heuristic Particle Swarm Optimization
MOPSO	Multi-objective Particle Swarm Optimization
MO-UDP	Multi-objective Uniformly Distributed Particles

NSGA	Non-dominated Sort Genetic Algorithm
PSO	Particle Swarm Optimization
PBDO	Performance Based Design Optimization
MOPBDO	Multi-objective Performance Based Design Optimization
QPSO	Quantum Particle Swarm Optimization
SBO	School Based Optimization



# CHAPTER 1

## INTRODUCTION

### 1.1 Structural Optimization at a Glance

With the world population approaching 8 billion, natural resources are rapidly being depleted and polluted. As far as the steel industry is concerned, numerous studies have been published investigating its impact on the environment caused by emitting various pollutants and consuming non-renewable energy sources (Burchart-Korol, 2013; Di Schino, 2019; Olmez et al., 2016; Tongpool et al., 2010). Considering that about half of the total steel production is used in the construction industry (T. Wang et al., 2007) for buildings (64%) and infrastructure (36%) (Moynihan & Allwood, 2012), engineers must adopt new ways to utilize steel more efficiently in the design of new structures, not only to reduce costs but also to preserve the nature.

Traditionally, structural design is an iterative process where an engineer or a group of engineers, based on experience, engineering judgment, and some preliminary analyses, determines the initial design configuration. Then, this configuration is analyzed, and if necessary, it is modified to satisfy the design requirements and reduce the cost. Generally, this sequence is repeated several times only until an acceptable solution is achieved. Thus, the resultant design is often not a cost-efficient one. However, if this old school trial-and-error approach is replaced by optimization tools and reformulated as an optimization problem, the design process can be automated to deliver code-compliant, cost-efficient designs.

An optimization problem has three fundamental elements. The first one is the objective function. In structural design optimization, the objective function is usually the structural weight, and it is tried to be minimized since the cost is directly associated with the amount of material used. The second element is the vector of

design variables. It defines the design configuration and may include one or more properties, such as member cross-sections, orientations of structural members, and joint locations. The third component consists of various constraints that must be satisfied. From the structural design point of view, constraints are the requirements imposed by design codes and construction practices.

There are three models for structural design optimization: (1) topology optimization, which aims to find the best distribution of materials in a structure through deciding the existence of structural elements; (2) shape optimization, which seeks to find the best geometry of a given structural system by determining locations of joints; (3) size optimization, which aims to find the best distribution of cross-sections for members of a given structural system, either by assigning any arbitrary (real-valued) section properties to members (continuous sizing optimization) or by selecting them from a discrete set of predefined sections (discrete sizing optimization).

In general, discrete sizing optimization is the only model applicable to steel frame structures since the topology and the shape are usually determined in the architectural design stage. Besides, the steel members must be selected and assigned from a set of commercially available steel profiles.

Once the structural optimization model is determined and the resultant optimization problem is formulated accordingly, an optimization method is selected to solve this problem at hand. Optimization methods that are used for structural optimization problems can broadly be classified into two categories as traditional mathematical techniques and modern metaheuristic techniques (Saka et al., 2016). The mathematical techniques can further be divided into two subcategories as mathematical programming methods and optimality criteria methods. These techniques require gradient information to guide the search process, which in turn makes them impractical for handling discrete optimization problems. Moreover, the quality of the optimum solution (final design) obtained with these methods is highly dependent on the starting point (initial design) of the optimization process such that usually, the search process converges to a local optimum nearest to the starting point.

Hence, if the optimization process is initiated from a poor design point, it may end up in a poor local optimum, which is very far from the global one. Thus, these methods are less likely to reach a global (or near-global) optimum, especially for complex design problems where numerous local optimum solutions may exist.

On the contrary, metaheuristics do not require gradient information or a good starting point. They can be applied to both discrete and continuous optimization problems. Given their inherent explorative capability all over the design space, they are also suitable for complex optimization problems. However, these techniques employ blind search strategies which are based on improving the best solutions obtained so far using random moves according to nature-inspired or swarm intelligence learning methodologies, and therefore they usually require a large number of function evaluations or response calculations, resulting in a slow convergence rate and an excessive amount of computing time. Even with the well-established algorithms of this category, depending on the size and complexity of the problem, at least several thousands of function evaluations are needed before reaching the global (or near-global) optimum (Hasançebi et al., 2009, 2010).

Several different strategies have been implemented to achieve a time-efficient optimization of large structures with metaheuristics. Some researchers (Hasançebi et al., 2011; Papadrakakis et al., 2003; Sarma & Adeli, 2001) adopted a parallel computing approach in which the computational work of structural analyses is distributed within a cluster of computers. Other researchers took advantage of artificial neural networks (ANNs) which are used to estimate structural response parameters of a structure, rather than implementing exact and time-consuming finite element analyses (Gholizadeh, 2015; Gholizadeh & Milany, 2016; A Kaveh et al., 2008; Papadrakakis et al., 1998) or constraint violations (Kaveh et al., 2012). Unfortunately, the former approach requires costly hardware set-ups, and the latter requires a sufficiently large and diverse training set. The size of the training set will be inordinate or even impractical for large-scale problems with a question on the accuracy of approximation.

An alternative and probably more effective way to solve structural optimization problems is to use analysis and design data to guide the optimization process. Such algorithms are referred to as design-driven optimization techniques. Early examples of these techniques include the well-known fully stressed design (FSD) and its extensions: fully utilized design (FUD) and modified fully utilized design (MFUD) (Patnaik et al., 1998). These algorithms may also be considered as variants of optimality criteria as they utilize a simple stress ratio (Kazemzadeh Azad, 2014). Although having a fast convergence rate, the fully stressed design method and its extensions may have some disadvantages. For example, FSD can only handle stress constraints. On the other hand, FUD can handle both stress and displacement constraints by prorating the FSD by a factor determined based on the most violated displacement constraint, yet it usually leads to overdesign solutions since structural elements may have different efficiencies in controlling a displacement constraint. MFUD provides improvements over FUD by using the Integrated Force Method (IFM) to identify critical members for each violated displacement constraint and, unlike FUD, applies different prorating factors for each member.

One of the recent extensions of FSD is the Fully Stressed Design Evolution Strategy (FSD-ES) (Ahrari & Atai, 2013; Ahrari & Deb, 2016), which combines the design-driven deterministic approach of FSD with global search capabilities of ES. It has been shown that this method demonstrates superior performance in comparison to other techniques, producing the best results for some selected benchmark optimization problems in the literature. Displacement constraints in this method are also handled by the utilization of the unit load method.

Another instance of the design-driven techniques is the fully constrained design (FCD) method (Flager et al., 2011), which utilizes the unit displacement method to map the global displacement constraint to each design variable in terms of strain energy density (SED). SED for each member is calculated and normalized by the highest SED to obtain SED ratios. Member stress and deflection constraints are also formulated as demand-to-capacity ratios. The optimization process is then guided based on the most critical constraint ratio of each design variable. It is important to



note that the numerical applications of MFUD, FSD-ES and FCD methods are limited to truss type structures.

Apart from MFUD, FSD-ES and FCD, the principle of virtual work has been employed for structural optimization problems with displacement constraints in many other studies (Chan, 2001; Elvin et al., 2009; Kazemzadeh Azad et al., 2014; Kazemzadeh Azad & Hasançebi, 2015; Park & Park, 1997; Walls & Elvin, 2010). Among these studies, guided stochastic search (GSS) (Kazemzadeh Azad et al., 2014; Kazemzadeh Azad & Hasançebi, 2015) is worth mentioning as it can handle multiple displacement constraints and is directly applicable (no sectional transformation) to discrete sizing optimization of both frame and truss type structures. In this method, the principle of virtual work is utilized to determine the displacement participation factor (DPF) of each member for all displacement constraints separately. When normalized by the volume, this factor gives a sensitivity index (SI) that represents the effectiveness of a member in satisfying a displacement criterion. Later, the search process is guided based on the SI values and information gathered from previous analyses and design calculations.

Another attempt is to develop hybrid metaheuristic techniques, where two or more algorithms are combined to produce an effective hybrid method that improves the computational speed and the quality of the optimum solution as compared to the cases where the techniques are implemented alone (Ting et al., 2015). Hybrid metaheuristic techniques have recently found applications in structural optimization literature; particularly in optimum design of trusses (Cheng et al., 2016; Kaveh et al., 2014; Kaveh & Ilchi Ghazaan, 2018; Kaveh & Mahdavi, 2015; Kaveh & Talatahari, 2012). Kazemzadeh Azad (2017) proposed several guided hybrid metaheuristic techniques, introducing a basic procedure based on member demand-to-capacity ratios for generating new candidate solutions, and reported significant computational savings particularly in the early stages of the optimization process.

## 1.2 An Overview of Performance Based Design

In conventional Force Based Design (FBD) codes, a structure is expected to endure service loads under various load combinations without showing excessive deformations or vibrations. Under seismic forces, the structure is allowed to go through inelastic deformations (i.e., plastic hinging) up to an acceptable limit. This is provided by means of a strength (force) reduction factor applied on the elastic response spectrum. Undesired failure modes or hinge formations are avoided by a prescriptive capacity design approach to ensure the ductility of the system. Although conventional force-based design codes generally yield satisfactory designs, there are some major problems as summarized in Priestley et al. (2007):

1. Period determination and distribution of design forces depend on initial stiffness estimates of structural members.
2. Even if initial stiffness is precisely known, the distribution of seismic forces based on initial stiffness is irrational as different structural members cannot be forced to yield simultaneously.
3. Unique force reduction factors (based on ductility capacity) consider structural type and material but do not reflect the geometry of different structural systems.

Consequently, the protection against earthquake damage changes significantly, even for the structures designed under the same code regulations. This is especially important if the questions about the life-cycle cost of a structure are concerned, e.g., under a particular seismic hazard, how much damage will occur? how much will be the repair cost? for how long the structure will be out of service, and what will be the associated cost? etc. These questions resulted in the emergence of a new design approach called the Performance Based Design (PBD) more than two decades ago. SEAOC Vision 2000 (1995), ATC-40 (1996), and FEMA-273 (1997) are the first guidelines which introduced the performance concepts into structural engineering. While SEAOC Vision 2000 was used for analysis and design for new buildings, and ATC-40 and FEMA-273 were introduced for seismic evaluation and rehabilitation

of existing buildings, both of them were later superseded by FEMA-356, ASCE 41-06, ASCE 41-13, and ASCE 41-17, respectively.

These guidelines suggest performance objectives for quantifying the seismic protection of existing structures. A performance objective is a pairing of a hazard level with a target structural performance level and a nonstructural performance level. A building is considered to attain a certain performance level, only if all its structural and nonstructural components satisfy the corresponding requirements of the related performance level (ASCE 41-13).

Mainly, there are three structural performance levels to define the post-earthquake damage state of a structure: immediate occupancy (IO), life safety (LS), and collapse prevention (CP). Immediate Occupancy is the damage state where a structure is safe to occupy, as it retains fundamentally all its pre-earthquake strength and stiffness. Life Safety level states that a structure is safe to occupy only after some structural repairs. Structural elements may suffer extensive damage, yet some protection margin is preserved against partial or total collapse. Life-threatening injury risk in this performance level is very low. Collapse Prevention level foresees significant loss in strength and stiffness of the lateral force-resisting system and poses partial collapse risk. The structure still supports the gravity loads but is on the verge of collapse and generally irreparable. Severe injury and life loss risk exist.

There are also performance levels defined for nonstructural components of a building as operational, position retention, and life safety levels. Operational level is the damage state where nonstructural components, after an earthquake, are expected to perform as the pre-earthquake state. Position Retention level states that the normal use of the structure might be interrupted, and some cleanup might be required. In general, building equipment functions properly if the utility service is provided. The risk of life-threatening injury caused by nonstructural damage is considered to be very low. Life Safety level is defined such that nonstructural components may be damaged, but the damage poses no threat to life safety. In some cases, nonstructural

performance may not be considered if reducing life-threatening risks might require the evaluation of structural components only (ASCE 41-13).

Performance evaluations of force-controlled and displacement-controlled structural components are processed separately. While force-controlled members are subject to some strength checks, deformation-controlled members are expected to meet specific plastic deformation limits corresponding to different performance levels. On the other hand, nonstructural components are subject to certain drift and strength limitations.

Reliable estimation of the engineering demand parameters in PBD requires using nonlinear analysis tools. In optimization studies, nonlinear static procedure (NSP), also known as pushover analysis, has usually been preferred over nonlinear dynamic procedure (NDP) for practical reasons. One reason behind this is that pushover analysis estimates seismic demands directly from the earthquake design spectrum, thus avoiding complications related to selection and scaling of ground motion records required for NDP (Reyes & Chopra, 2011). Secondly, NSP requires much less execution time in comparison to NDP. On the other hand, conventional pushover analysis, which has a single invariant lateral load pattern proportionate to fundamental mode shape, may provide misleading results if (1) higher-mode effects are significant or (2) a structure suffers from considerable stiffness degradation under seismic action such that its dynamic characteristics are altered, and initial lateral load pattern based on elastic mode shape becomes invalid. Many different variants of pushover analysis have been proposed to extend the application of pushover analysis to such cases mostly through the utilization of multi-modal and adaptive load patterns (Chopra et al., 2004; Chopra & Goel, 2002; Elnashai, 2001; Gupta & Kunnath, 2000; Hernández-Montes et al., 2004; Kaatsız & Sucuoglu, 2014; Kalkan & Kunnath, 2006; Kreslin & Fajfar, 2012; Reyes & Chopra, 2011; Soleimani et al., 2017; Sucuoglu & Günay, 2011). Nonetheless, none have been proven to be universally applicable, and standardized as a reliable alternative to NDP. In fact, some of these procedures are more complicated than NDP and contradicts with the original purpose of NSP, being a simple method for checking potential weaknesses

of new or existing structures (Baros & Anagnostopoulos as cited in Kreslin & Fajfar, 2012).

In recent ASCE 41-13 and ASCE 41-17 guidelines, the use of pushover analysis method is limited to structures without significant higher-mode effects and stiffness degradation, and a lateral load pattern proportional to fundamental mode shape in the direction under consideration is recommended.

Currently, there is no building code with a complete performance-based design approach. All of the performance-based guidelines discussed earlier in this section are either for evaluation and rehabilitation purposes of existing buildings or merely design recommendations. Over the last two decades, many researchers have shown increasing interest in adopting these guidelines to the design of new buildings under structural optimization framework.

In the next section, a critical review of the state-of-the-art in **performance-based design optimization (PBDO)** of steel moment frames is outlined.

### **1.3 PBDO of Steel Moment Frame Structures: A Critical Review of the State-of-the-Art**

As discussed previously in the preceding section, currently, there is no performance-based design code in practice. On the other hand, there is a consensus on the performance-based optimum design methodology for steel moment frame structures in the literature. This methodology considers two stages of design checks. In the first stage, the serviceability of structure under non-seismic load combinations is verified by linear static analysis. Then in the next stage, the seismic performance of the structure under a particular seismic hazard or a set of hazard levels is assessed by nonlinear analysis tools.

The vast majority of PBDO studies shown in Table 1.1 adopted inter-story drift ratio (IDR) as the only performance parameter to measure seismic performance and disregarded plastic deformation limits. This, to a certain extent, can be justified

because inter-story drift is a good measure of both structural and nonstructural damage since it is closely related to plastic rotation demands in beam-column connections (FEMA-350). From the optimization point of view, the main tendency for incorporating only the inter-story drift (or any other global performance criterion) lies in the fact that it significantly reduces the computational burden during the optimization process. Instead of satisfying performance constraints separately for each structural component in a story, their performance is handled roughly as a whole by limiting the inter-story drift.

Table 1.1 An overview of studies on PBDO of steel moment frames

#	Publication	Analysis Method	Performance Parameter	Objective Function(s)	Optimization Algorithms
1	Liu et al. (2005)	Pushover (height-wise)	IDR	Weight vs. Max. IDR	MOGA
2	Fragiadakis et al. (2006)	Pushover (1 <sup>st</sup> Mode)	IDR	Weight vs. LCC	ESMO
3	A. Kaveh et al. (2010)	Pushover (height-wise)	Roof Drift	Weight	ACO
4	A. Kaveh et al. (2012)	Pushover (1 <sup>st</sup> Mode)	IDR	Weight vs. LCC	NSGA-II
5	Gholizadeh et al. (2012)	Pushover (height-wise)	IDR	Weight	GA, ACO, HS, PSO
6	Li et al. (2012)	Pushover (MMPA)	IDR	Weight vs. LCC	ASA
7	Gholizadeh & Moghadas (2014)	Pushover (height-wise)	IDR	Weight	QPSO, IQPSO
8	A. Kaveh & Nasrollahi (2014)	Pushover (height-wise)	Roof Drift	Weight	CSS
9	K. Mohammadi & Ghasemof (2015)	Pushover (1 <sup>st</sup> Mode)	Local EDPs	Weight	UDT method
10	Gholizadeh (2015)	Pushover (height-wise)	IDR	Weight	MFA
11	Liang et al. (2015)	Pushover (MPA)	IDR	Weight vs. Roof Drift	NSGA-II, MOPSO, MGSO, MOHPSO
12	Gholizadeh & Milany (2016)	NTHA	IDR	Weight	DEO, ECBO, ECBO-II, PSO
13	Gholizadeh & Baghchevan (2017)	Pushover (height-wise)	IDR	Weight vs. Max. IDR	CMOFA
14	Mokarram & Banan (2018)	Pushover & NTHA	IDR	Weight vs. LCC	FC-MOPSO
15	Gholizadeh & Fattahi (2019)	IDA	Roof Drift	Weight vs. ODI	MO-UDP
16	Wang et al. (2020)	NTHA	Local EDPs, IDR	Weight	UDT method (two-fold strategy)
17	Degertekin et al. (2020)	Pushover (height-wise)	IDR	Weight	SBO

The inter-story drift limits given in FEMA-273 and FEMA-356 for expected damage states based on structural type and material have been frequently used in PBDO studies. However, FEMA-356 underlines that these limits are only illustrative and do not supersede member or component level performance limits. In fact, a design based solely on the inter-story drift limits cannot guarantee that member/component performance limits are satisfied as well. Plastic rotation demands can vary significantly from one member to another even under the same inter-story drift ratio (Eom et al., 2013).

The major challenge of PBDO problems is extremely long and sometimes prohibitive computation time associated with the large number of nonlinear analyses performed during the optimization process by metaheuristic techniques. It is not surprising that numerical examples in most studies are limited to planar models, which can significantly reduce the size of the optimization problem. Similarly, pushover analysis is almost always the preferred method of analysis for evaluating structural performance since its alternative, NDP, is much more time-consuming. However, it should be noted that planar models are more suitable for regular plan buildings, and the application of pushover analysis has some limitations as discussed in the previous section.

Unlike metaheuristics, design-driven search techniques have only a very limited number of applications in the PBDO problems because most of these techniques are based on the virtual work principle (see Ch. 1.1) and thus not applicable to performance-based design optimization (PBDO) problems, where structural performance is assessed by nonlinear analysis tools. However, some design-driven optimization algorithms based on uniform deformation theory (UDT) are presented for PBDO problems in the literature. Mohammadi and Ghasemof (2015) developed a UDT-based optimization technique for PBDO of planar steel frames with member level performance objectives. This technique utilizes imaginary cross-sections to turn the discrete sizing optimization problem into a continuous one where the plastic section modulus is the only design variable. These sections are modified and transformed into the nearest discrete section to approach a more uniform deformation

distribution gradually at each iteration step. The results demonstrate a much higher convergence rate compared to several metaheuristics. However, in its proposed state, the algorithm has no strategy for handling displacement constraints, making it impractical for real design scenarios. Wang et al. (2020) proposed another optimization algorithm based on UDT and imaginary cross-sections. Although this method takes displacement constraints into account, the numerical examples are limited to planar frames only. Besides, since this method requires transforming the imaginary sections into real discrete sections at the end of the optimization, it is questionable whether a feasible solution can be found in terms of geometric (constructability) constraints, especially for space frames, which have much complex connections.

In a multi-objective performance-based design optimization (MOPBDO) problem, the cost and performance of a design are treated as two competing objectives. Generally speaking, in structural optimization problems, there exists almost an infinite number of feasible design alternatives in the search space. Some of these designs are inferior to others in terms of both cost and performance. When these inferior designs are eliminated, the remaining set of designs are mathematically referred to as the pareto optimal set. Any design in a pareto optimal set is superior to another by either cost or performance but not both, implying that there is always a trade-off between cost and performance from one design to another (non-dominancy). However, finding the pareto optimal set in multi-objective optimization problems is not an easy task, and for complex problems it is only an approximation formed by a set of non-dominated solutions retrieved during the optimization process (near pareto optimal set). For a decision maker, the meaning of pareto optimal set is a list of alternatives from which one can choose among the cost-efficient designs with varying performance levels.

Performance related objective function of the MOPBDO problems is generally chosen as maximum inter-story drift ratio (Gholizadeh & Baghchevan, 2017; Liu et al., 2005) or life-cycle cost as an implicit function of inter-story drift ratio (Fragiadakis et al., 2006; Ali Kaveh et al., 2012; Mokarram & Banan, 2018). In these



studies, life-cycle cost (LCC) function and drift ranges (corresponding to damage states given in ATC-13) are based on the work by Wen & Kang (2001a, 2001b), and the cost ratios (damage factors) expressed as a percentage of the replacement cost are taken from ATC-13.

Cost ratios can be determined by empirical studies on the field data collected after earthquakes or by expert opinion. They may show significant variations depending on the site or location. They provide approximate estimations of the replacement costs and are especially useful when more accurate information is not available (Hill & Rossetto, 2008). It should also be noted that while the damage states and the corresponding cost ratios are discrete, the inter-story drift ratios can assume any values, making the LCC predictions even less accurate. Some researchers adopted fuzzy-decision theory to make the cost ratios continuous over the range of inter-story drift index (Li et al., 2012; Zou et al., 2007).

Different from the above approaches, Gholizadeh & Fattahi (2019) used a modified version of the overall Park-Ang damage index (Ghosh et al., 2011), as the performance criterion of the MOPBDO problem. Basically, this index was formed by the ratio of inelastic demand-to-capacity ratio of the roof displacement plus the absorbed hysteretic energy.

While designing a new structure in accordance with PBD methodology, through nonlinear structural analysis, not only global demand parameters such as inter-story drift ratios or roof displacements are estimated, but also the local engineering demand parameters (EDP) such as plastic rotations of deformation-controlled members and stresses in force-controlled members are obtained, which provides valuable information to assess the performance of the structure more accurately. Similarly, more accurate LCC estimations can be made if these local EDPs are explicitly considered rather than abovementioned approximations based only on global demand parameters.

In the light of the discussions in this section, the following conclusions can be derived:

- 1) A reliable performance-based design methodology cannot be established considering only a single performance parameter, such as inter-story drift. Rather, local performance parameters such as plastic rotations must also be considered during the design stage.
- 2) Metaheuristics might be impractical to use for computationally expensive PBDO problems due to their slow convergence rates.
- 3) The use of a design-driven optimization algorithm is recommended for PBDO problems due to their relatively fast and improved convergence abilities, yet the algorithm employed must handle not only the local stress and deformation constraints but also the global displacement and geometric constraints effectively if the real design applications are targeted.
- 4) In MOPBDO problems, a more meaningful cost-performance trade-off relationship can be established if the hierarchy among alternative designs are determined by consideration of the local performance parameters and the distribution of the damage over the entire structure.

#### **1.4 Aim and Scope of the Thesis**

The objectives of this study can be summarized as below:

- 1) Developing a fast and efficient design-driven optimization algorithm that can be applied effectively to solve optimum design problem of steel structures according to both FBD and PBD methodologies.
- 2) Providing a cost and seismic performance comparison of optimally designed structures under FBD and PBD methodologies.
- 3) Presenting the cost-performance trade-off relationship among the alternative designs under MOPBDO framework.

The organization of the chapters is as follows:

Chapter 2 presents a mathematical formulation for the discrete sizing optimization of steel frame structures designed according to conventional FBD and PBD

methodologies. Therein, the design constraints and load combinations are also provided with reference to related design codes and guidelines. In Chapter 3, a novel design-driven optimization method called Capacity Controlled Search (CCS) is proposed by presenting its working mechanism and detailed algorithm. In Chapter 4, the performance of the CCS algorithm is numerically investigated by solving several optimum FBD problems featuring various 2D and 3D ordinary moment resisting steel frames and compared with those of two well-established metaheuristic search techniques in terms of computational efficiency, quality of the optimum solution, and reliability of the solutions obtained in individual runs. In Chapter 5, the same steel frames from the previous chapter are this time optimized according to PBD methodology. Then, a comparison of optimally designed structures under conventional FBD and PBD methodologies is presented in terms of design cost and seismic performance. Chapter 6 describes a simplified approach for MOPBDO by the CCS technique and presents the alternative PBD solutions obtained by this approach. Finally, Chapter 7 concludes the thesis by providing key findings in this study and recommendations for future research.



## CHAPTER 2

### PROBLEM FORMULATION

#### 2.1 Design Variables and Objective Function

The total construction cost of a steel structure depends on a number of cost items, including material, manufacturing, transportation, and erection costs. Even though the minimum design weight of a structure does not guarantee the lowest cost of a structure, it is a common practice in structural optimization to minimize the structural weight since it is a good measure of the material cost.

As remarked in the previous chapter, the discrete sizing optimization refers to the case where the design variables (member sizes) are selected from a predefined set of sections often referred to as discrete set or section pool. Hence, before optimum design process is initiated, it is necessary to prepare a section pool where discrete sections are sorted in ascending or descending order of some sectional properties, such as cross-sectional area or moment of inertia, etc. In a section pool each discrete section is designated by a different sequence (index) number that varies between 1 to total number of discrete values in the section pool. For instance, if there are 82 discrete sections in the section pool, each discrete section is assigned to a different sequence number between 1 and 82. For a design variable, the selection of a discrete value from the section pool is carried out in conjunction with sequence numbers. That is to say, once a selection is carried out for a design variable, the cross-sectional properties of each section become available from the section pool.

For a steel structure with  $N$  members, assuming that the steel members are grouped into  $N_g$  design variables (members groups) for the purpose of practicality and constructability, the optimization problem concerning the minimum weight design of a steel structure can be stated as follows:

The objective is to find a vector of design variables  $\mathbf{I}$ ,

$$\mathbf{I}^T = [I_1, I_2, \dots, I_{N_g}] \quad (2.1)$$

which minimizes the weight ( $W$ ) of a structure,

$$W = \sum_{i=1}^{N_g} \gamma_i A_i \sum_{j=1}^{N_m} L_j \quad (2.2)$$

In Equations (2.1) and (2.2), the design variable vector  $\mathbf{I}$  holds the sequence numbers of  $N_g$  member groups from the section pool, which is usually constructed from selected AISC standard wide-flange steel sections,  $\gamma_i$  and  $A_i$  are the unit weight and area of a standard section adopted for a member group  $i$  respectively,  $N_m$  is the total number of members in group  $i$ , and  $L_j$  is the length of the member  $j$  of the group  $i$ .

The design constraints consist of a set of behavioral requirements imposed according to provisions of a selected design code as well as geometrical restrictions. The design constraints of steel structures according to FBD and PBD methodologies are formulated separately in the subsequent sections of this chapter.

## 2.2 Design Constraints of FBDO Problem

In compliance with LRFD methodology in ANSI/AISC 360-10 design code, the following strength requirements are considered for the design of the structural steel members:

- (1) For members subjected to combined axial load and bending:

$$g_1 = \left(\frac{P_r}{P_c}\right)_j + \frac{8}{9} \left(\frac{M_{rx}}{M_{cx}} + \frac{M_{ry}}{M_{cy}}\right)_j - 1.0 \leq 0 \quad \text{for} \quad \left(\frac{P_r}{P_c}\right)_j \geq 0.2 \quad (2.3)$$

$$g_1 = \left(\frac{P_r}{2P_c}\right)_j + \left(\frac{M_{rx}}{M_{cx}} + \frac{M_{ry}}{M_{cy}}\right)_j - 1.0 \leq 0 \quad \text{for} \quad \left(\frac{P_r}{P_c}\right)_j < 0.2 \quad (2.4)$$

(2) For members subjected to shear:

$$g_2 = \frac{V_{r,j}}{V_{c,j}} - 1 \leq 0 \quad (2.5)$$

where  $P_r$ ,  $M_r$ , and  $V_r$  are the required axial, flexural, and shear strength demands calculated using LRFD load combinations, respectively;  $P_c$ ,  $M_c$ , and  $V_c$  are the axial, flexural, and shear strength capacities determined in accordance with AISC 360-10 LRFD provisions, respectively;  $x$  and  $y$  are the subscripts which represent the strong and the weak axis of bending for a member, respectively; subscript  $j = 1, 2, \dots, N_t$  denotes the  $j^{\text{th}}$  member of the structure, where  $N_t$  is the total number of structural members.

For the deflection of beams subjected to reduced live load, the traditional “1/360” limit in practice is adopted and formulated as a design constraint as follows:

$$g_3 = \delta_j - \frac{L_j}{360} = \frac{360\delta_j}{L_j} - 1 \leq 0 \quad (2.6)$$

where  $\delta_j$  and  $L_j$  are the calculated deflection in a beam and its corresponding length, respectively; the subscript  $j = 1, 2, \dots, N_b$  denotes the  $j^{\text{th}}$  member of the structure, where  $N_b$  is the total number of beam elements.

In compliance with ASCE 7-10 design load specifications, the inter-story drift under seismic action is limited as follows:

$$g_4 = \frac{\Delta_i}{\Delta_a} - 1 \leq 0, \quad \text{where} \quad \Delta_i = \frac{C_d \delta_{xe}}{I_e} \quad (2.7)$$

In Equation (2.7),  $\Delta_i$  and  $\Delta_a$  represent the drift of the  $i^{th}$  story and its allowable design story drift, respectively;  $\delta_{xe}$  is the maximum difference between the horizontal displacements of vertically aligned points at the top and bottom of a story along any of the edges of the structure and is determined by the elastic analysis as;  $C_d$  and  $I_e$  are the deflection amplification factor and the importance factor, respectively. The subscript  $i = 1, 2, \dots, N_s$  denotes the  $i^{th}$  story, where  $N_s$  is the total number of stories.

It should be noted that steel members require special connection requirements. If these requirements are disregarded during the design phase, the resulting design will not be practical from the constructability point of view. Hence, it is crucial that the following geometric constraints (Figure 2.1) are considered for the connections between different members:

(1) For column-to-column connections:

$$g_5 = \frac{h_{upper}^c}{h_{lower}^c} - 1 \leq 0 \quad (2.9)$$

(2) For beams connecting to column flange:

$$g_6 = \frac{b_f^b}{b_f^c} - 1 \leq 0 \quad (2.10)$$

(3) For beams connecting to column web:

$$g_7 = \frac{b_f^b}{(h^c - 2t_f^c)} - 1 \leq 0 \quad (2.11)$$

where  $h$ ,  $b_f$ , and  $t_f$  are the section depth, flange width, and flange thickness of the doubly symmetric steel section assigned to a structural element, respectively; and the superscripts  $b$  and  $c$  denote the corresponding beam and column element, respectively.



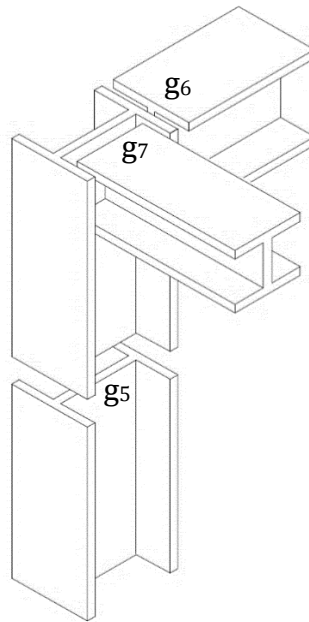


Figure 2.1. Geometric (constructability) constraints

The following load combinations are considered for the numerical examples in this study, as specified in ASCE 7-10, Section 2.3:

- (1)  $1.4D$
- (2)  $1.2D + 1.6L$
- (3)  $1.2D + 1.0L \pm 1.0E$
- (4)  $0.9D \pm 1.0E$

where  $D$ ,  $L$ , and  $E$  represent the dead, live, and earthquake loads, respectively.

### 2.3 Design Constraints of PBDO Problem

As previously discussed, the PBD methodology requires two stages of design checks. In the **first stage**, it is checked and ensured that all constraints given in the previous section for the FBD methodology are satisfied under non-seismic load combinations only. On the other hand, the **second stage** design constraints are introduced to ensure a satisfactory seismic performance of a structure under a specified hazard level or a

set of hazards. Only the second stage design constraints are presented in this section to avoid repetition.

In this study, the pushover analysis method with a lateral load pattern based on fundamental mode shape in the direction under consideration is conducted to assess the seismic performance of the structures. All the design constraints in this section are accordingly adapted from ASCE 41-13.

The deformation-controlled members of steel moment-resisting frames (SMRFs) are subject to the following constraint:

$$g_1 = \frac{(\theta_p)_j}{(\theta_a)_j} - 1 \leq 0 \quad (2.12)$$

where  $\theta_p$  is the plastic rotation of a hinge at the target displacement, and  $\theta_a$  is the corresponding allowable plastic rotation for the targeted performance level (IO, LS, or CP); the subscript  $j = 1, 2, \dots, N_h$  denotes the hinge  $j$ , where  $N_h$  is the total number of hinges defined on the deformation-controlled members.

The members subjected to compressive forces in the excess of 50% of its axial load carrying capacity are designated as force-controlled members, and they must satisfy the following constraint:

$$g_2 = \left( \frac{P_t}{P_{CL}} + \frac{M_{tx}}{M_{CLx}} + \frac{M_{ty}}{M_{CLy}} \right)_j - 1 \leq 0 \quad (2.13)$$

where  $P_t$  and  $M_t$  are the axial load and bending moment capacities at the target displacement, respectively;  $P_{CL}$  and  $M_{CL}$  are the lower bound compressive and flexural strengths, respectively;  $x$  and  $y$  are the subscripts which represent the strong and the weak axis of bending for a member, respectively; the subscript  $j = 1, 2, \dots, N_f$  denotes the  $j^{th}$  force-controlled member of a structure where  $N_f$  is the total number of the force-controlled members.

The following constraint on the inter-story drift is also considered for limiting damage to nonstructural components at the target displacement:

$$g_3 = \frac{\Delta_i}{\Delta_a} - 1 \leq 0 \quad (2.14)$$

In Equation (2.14),  $\Delta_i$  and  $\Delta_a$  represent the drift of the  $i^{th}$  story and its allowable design story drift, respectively;  $\Delta_i$  is the maximum difference between the horizontal displacements of vertically aligned points at the top and bottom of a story at the target displacement. The subscript  $i = 1, 2, \dots, N_s$  denotes the  $i^{th}$  story, where  $N_s$  is the total number of stories.

In nonlinear static analysis, the actions caused by seismic forces are considered under the following combination of gravity loads ( $Q_G$ ), as specified in ASCE 41-13, Section 7.2:

$$Q_G = Q_D + Q_L \quad (2.15)$$

where  $Q_D$  and  $Q_L$  are the actions caused by dead loads and live loads, respectively.  $Q_L$  is taken equal to 25% of the unreduced live load in accordance with ASCE 7-10 but cannot be taken less than the actual live load.

## 2.4 Penalized Objective Function

The objective function given in Equation (2.2) refers to the unconstrained objective function of the problem at hand. However, in the case where the solution space is restricted by design constraints, this function should be modified in a way to handle problem constraints as well. Usually, this is achieved through the use of penalty functions where the designs violating the problem constraints are penalized and their objective functions are calculated using the following equation:

$$\phi = W[1 + Penalty(\vec{a})] = W[1 + r(\sum_{j=1}^{N_c} \max(0, g_j))] \quad (2.16)$$

In Equation (2.16),  $\phi$  and  $W$  represents the penalized (constrained) objective function and the unconstrained objective function, respectively; the subscript  $j = 1, 2, \dots, N_c$  denotes the  $j^{th}$  normalized design constraint, where  $N_c$  is the total number of constraints on the design. The penalty coefficient  $r$  is used to adjust the intensity of penalization as a whole. This parameter can be either set to a static value, which is usually taken as 1.0 or adjusted dynamically during the course of optimization process. In this study, the former approach is adopted.

## CHAPTER 3

### CAPACITY CONTROLLED SEARCH TECHNIQUE

In this chapter, a novel design-driven optimization technique called Capacity Controlled Search (CCS) is introduced for discrete sizing optimization problems of frame type structures with single or multiple displacement constraints. In the following sections, first, the working mechanism of this technique is explained, and then its detailed algorithm is presented.

#### 3.1 The Working Principle of CCS

The main idea behind the CCS technique lies in the effective utilization of structural components while resisting design loads. A structural component is locally subjected to stress and displacement constraints to ensure safety and serviceability requirements. In addition, every structural component contributes -with varying levels- in satisfying a global displacement criterion, such as inter-story drift or roof drift.

In the absence of a global displacement criterion, a fully stressed design or in a broader sense, a fully utilized design, where each structural component is used at its utmost member strength and/or displacement capacity, generally results in cost-efficient designs. However, in practical design applications, there are often global displacement criteria that must be satisfied by an acceptable design.

As discussed in the first chapter, the design-driven optimization techniques in the literature rely on the use of unit load method for determining the efficiency of structural elements to satisfy a global displacement criterion. Although these algorithms have proved to be very effective in structural sizing optimization problems, their use is limited to only conventional force-based design problems. The

fact that nonlinear force-deformation models are used to define the behavior of a structural component in a performance-based design problem, does prevent the use of unit load method and its variants for such problems.

The CCS technique, on the other hand, can be applied to both force-based and performance-based design problems with or without displacement constraints. It does not require any pre-analysis such as unit load method to determine the efficiency of structural elements in satisfying displacement criteria, but rather assumes a probabilistic approach to retreat from an infeasible search direction.

In the CCS method, ideally, the design process is initiated by assigning the largest available section sizes to all member groups (design variables). Then, this initial design configuration is analyzed under all design load combinations, and the maximum demand-to-capacity ratio (DCR) for each member group is determined by considering both local stress and displacement (deflection, plastic rotation) constraints. The design variables to be modified are selected probabilistically based on DCR values in a way such that the member group with the lowest DCR has the highest chance for selection and vice versa. The rationale here is to push the member groups with low DCRs to their limits by selecting somewhat smaller sections for them in order to achieve a uniform demand distribution within the structure as much as possible. Indeed, at the beginning of the optimization process, most member groups are likely to have low DCR values because initially the member groups are assigned to the largest available section sizes. Hence, most of the design variables, if not all, are selected and modified in the early stages of the optimization process, leading to an effective explorative search of the design space. However, as the iterations continue and the better solutions are produced in the course of optimization, DCRs of member groups will increase. Accordingly, a lesser number of design variables will be chosen and modified, implying that the exploitative capability of the algorithm will increase gradually while the explorative capability is slowly reduced.

Once the selection phase is completed, selected design variables are perturbed based on some probabilistic rules. A member group with a DCR higher than 1.0 means that it fails to satisfy a design constraint and a stronger section must be assigned. On the other hand, if its DCR is less than unity, a smaller section can be assigned to provide economy. However, as previously argued, some structural components with lesser utilization ratio might have a predominant effect on the global displacement criterion such that even a stronger section might need to be assigned for such members. Likewise, changing the sizes of some member groups in indeterminate structural systems may lead to overall force distributions such that not only the changed member groups are affected by this redistribution but also the unchanged member groups. For instance, for a member with a DCR greater than unity, when the size of a different member group is changed, the member in consideration (although not changed) may now be subjected to lesser loads, resulting in a DCR less than 1.0. For these reasons, The CCS technique employs a simple probabilistic approach (via  $\beta$  parameter, which will be introduced in the next section) while deciding whether a stronger or smaller section will be assigned to a member group. In this approach, a member group with a DCR value greater than 1.0 is given a greater chance to be assigned to a stronger section; yet the possibility that the group might be assigned to a smaller section still exists but with a lesser probability. Conversely, a member group with a DCR value less than 1.0 is given a higher chance to pick a smaller section, but a stronger section might also be assigned with a reduced possibility. The selection and perturbation phases are repeated over a predefined number of iterations or a termination criterion for the optimization algorithm is satisfied.

The terms “stronger” and “smaller” sections used in the CCS algorithm require particular attention and explanation. It is important to emphasize that to implement the CCS algorithm all available steel sections in a section pool (discrete set) are sorted in ascending order of cross-sectional areas. It is relatively easy to define “the smaller section”, because it simply corresponds to a section with a lesser cross-sectional area amongst any given two sections. However, when it comes to defining a stronger section, this identification may not be that straightforward because

multiple failure modes are usually available for structural members. For example, one member may fail under shear forces, another member may fail under bending in the stronger axis or weak axis, or local buckling mechanisms may be observed. If in an optimization process the evaluations of designs are not carried out internally using an integrated finite element method, rather an external structural analysis software is used, then such information may not always be made available by the software or it may be uneasy to derive from the analysis results which mechanism actually caused the failure of the structural member under consideration. In such cases, it is not possible to define the stronger section without making gross assumptions. One may think to choose a section having a larger cross-sectional area and moment of inertias in both bending axes than the currently assigned one, which in turn eliminates the need for identifying the failure mode. However, by doing so the sections in between will be omitted even though they might have adequate strength as well depending on the failure mode. On the other hand, it is still plausible to assume a correlation between the cross-sectional area and moment of inertias in about both axes of bending. This simplifies and transforms the definition of “stronger section” into “larger section” at the cost of discarding smaller sections with adequate strength depending on the failure mode. However, the probabilistic perturbation scheme of CCS mentioned previously will also take part in here to detect the “smaller but still stronger” sections by preserving a chance to pick smaller sections for member groups with DCRs greater than unity (i.e., failing a strength/displacement constraint).

The CCS algorithm also utilizes a basic **stagnation control strategy** based on **uphill move** to avoid being stuck at a local optimum solution. If the best solution is not improved over a predetermined number of iterations, the algorithm starts a stagnation escape period (SEP). In SEP, the elitism rule that the design transition is only allowed to better solutions is suspended temporarily and the transition to a non-improving solution (uphill move) is allowed provided that it has a penalized weight (constrained objective function value) not more than a predefined ratio ( $\alpha$ ) of the penalized weight of the elite design. Once the elite design is replaced with a non-improving design, candidate designs are generated from this non-improving design (temporary elite



design), and the elitism rule is activated again. Whenever a solution better than the temporary elite design is generated, it replaces the temporary elite design, and hence the following designs are produced from this new temporary elite design. On the other hand, if a solution better than the elite design is located, it replaces the elite design; and SEP is terminated immediately. If no improvement is achieved within the SEP, another SEP loop is started but this time uphill move is performed with reference to the last temporary elite design of the previous SEP.

The CCS algorithm also takes advantage of the well-known upper-bound strategy (UBS) (Kazemzadeh Azad et al., 2013) to reduce the computational burden of structural analyses required during the optimization process. It should be noted that the proposed CCS algorithm implements a strict elitism rule, in which a candidate design could beat and replace the current design only if it is better than the latter, and thus is very suitable for UBS. The UBS suggests that candidate designs with structural weights greater than the objective function value (penalized weight,  $\phi$ ) of the elite design have no chance to improve the elite design and hence such designs can automatically be skipped without a need to perform time-consuming structural analyses for them. That is to say, every design generated in the course of optimization is first checked for its structural weight, and the structural analysis is implemented only if its structural weight is lower than the objective function ( $\phi$ ) of the elite design; otherwise, this design is eliminated without performing structural analysis, which in turn leads to considerable savings in computational time of the algorithm. In the present study, the basic UBS approach is further improved such that not only the weight but also the constraints (e.g., geometric constraints) that can be calculated without a need for structural analysis are used to calculate the penalized weight of a candidate design prior to the structural analysis, called pre-analysis objective function. A candidate design is analyzed only if its pre-analysis objective function is lower than the objective function of the elite design. This way even more candidate designs can be eliminated without performing structural analysis and substantial computational savings can be achieved. It is also possible to implement the UBS dynamically during different phases of structural analyses. For example, after

determining local response constraints (e.g., stresses, deflections, etc.) first, the penalized weight of a candidate design weight is updated and checked whether it is still able to improve the elite design. If it is not, later phases of structural analyses like determining story drift ratios or hinge states (if it is PBDO) can be skipped to avoid unnecessary computations. This version of UBS proposed within the context of this study is referred to as **improved upper-bound strategy (iUBS)**.

### 3.2 CCS Algorithm

In the previous section, the idea behind the CCS method has been elaborated. In this section, the detailed algorithm of CCS is provided.

#### Step 1: Initiation

The steel sections in discrete sets (section pools) are sorted in ascending order of their cross-sectional areas prior to optimization. The initial design is ideally formed by assigning the largest available sections to each member group. Then, this initial design is analyzed, and its penalized weight is calculated. The DCR of each member group is also recorded for the selection phase. The iteration number is set to 1.

#### Step 2: Selection

Based on the DCR of each member group, the variables to be perturbed for generating a candidate design is selected by the following probabilistic formula:

$$\max(P_{min}, |1 - DCR_i|^u) \geq Rand_i \quad (3.1)$$

If the above inequality is satisfied for a design variable, then it is selected for perturbation. In this equation,  $P_{min}$  is the minimum selection probability;  $u$  is the uniformity coefficient; the subscript  $i = 1, 2, \dots, N_g$ , denotes the  $i^{th}$  member group

(design variable), where  $N_g$  is the total number of member groups.  $Rand_i$  is a uniformly distributed random number between 0 and 1.

### Step 3: Perturbation

Perturbation of a design variable is conducted by stochastically assigning a new steel section within a search neighborhood. The width of a search neighborhood can be defined according to one of the following three schemes:

1. Constant search neighborhood width ( $nw_c$ ):

$$nw_{c,i} = \text{round}(\sqrt{N_{sec,i} - 1}) \quad (3.2)$$

2. Linearly decreasing search neighborhood width ( $nw_d$ ):

$$nw_{d,i} = nw_{c,i} - (nw_{c,i} - 1)(iter/iter^{max}) \quad (3.3)$$

3. Adaptive search neighborhood width ( $nw_a$ ):

$$nw_{a,i} = nw_{c,i}(\min(1, \text{abs}(1 - DCR_i)))^\rho \quad (3.4)$$

$$nw_{min} \leq nw_{a,i} \quad (3.5)$$

In Equations (3.2)-(3.5),  $N_{sec,i}$  is the number of available sections in the section pool associated with the member group  $i$ ;  $DCR_i$  is the maximum demand-to-capacity ratio of the  $i^{th}$  member group under all load combinations;  $iter$  and  $iter^{max}$  are the current iteration number and a predefined maximum iteration number, respectively;  $\rho$  is a parameter used to adjust the rate of reduction in the search neighborhood width; and  $nw_{min}$  is the minimum search neighborhood width. Figure 3.1 illustrates the change in normalized  $nw_a$  with respect to varying levels of DCR.

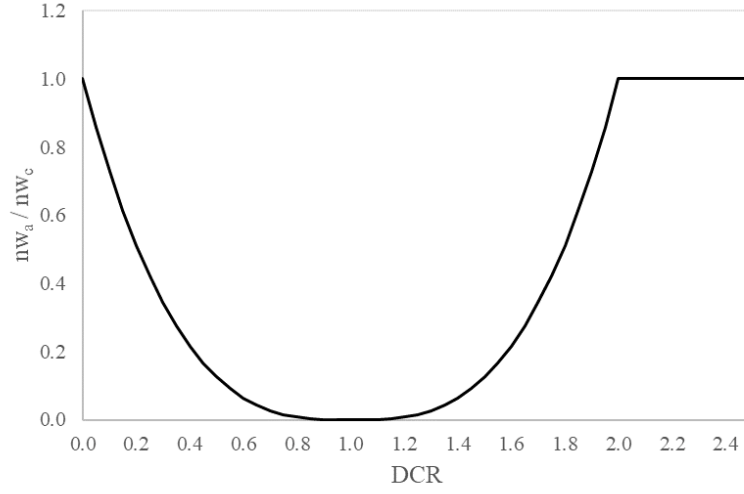


Figure 3.1. Adaptive search neighborhood width

A new section within the search neighborhood ( $nw_{x,i}$ ) is then assigned to a selected member group by the following formulas:

$$I_i^{iter+1} = I_i^{iter} + \text{round}(\beta \cdot \max(1, \text{abs}(\text{Rand}n_i) \cdot nw_{x,i})) \quad (3.6)$$

$$\beta = \text{sign}((DCR_i - 1)(\tau - \text{Rand}_i)) \quad (3.7)$$

where  $I_i$  is the sequence (index) number of the steel section currently assigned to the selected design group;  $\beta$  is a probabilistic parameter which decides whether a larger or smaller section will be assigned to the selected design group;  $\tau$  is a constant used to adjust  $\beta$ ;  $\text{Rand}n_i$  is a normally distributed random number with zero mean and standard deviation of one;  $\text{Rand}_i$  is a uniformly distributed random number between 0 and 1.

#### Step 4: Analysis & Evaluation

The pre-analysis penalized weight (objective function) of the candidate design is calculated. If this value is higher than the objective function value of the elite design,

the candidate is automatically rejected; otherwise, it is allowed to go through the structural analysis phase to obtain the force and deformation responses, and the final penalized weight of the candidate design is calculated. If the candidate design has a lower penalized weight than that of the elite design, it replaces the current design and becomes the new elite design. Otherwise, it is rejected.

#### **Step 5: Stagnation Control**

If the best solution is not improved over a predetermined number of iterations, SEP is initiated. If an ongoing SEP is active and the best solution is improved in the previous step, SEP is terminated.

#### **Step 6: Termination**

If a termination criterion is satisfied (i.e., reaching a predefined maximum iteration number, etc.), the iterations are stopped. Otherwise, the iteration number is increased by 1, and the steps 2-6 are repeated.



## CHAPTER 4

### VERIFICATION OF THE CCS TECHNIQUE

#### 4.1 Numerical Examples

The performance of the proposed CCS algorithm is numerically investigated by solving four optimum design problems featuring various 2D and 3D ordinary moment-resisting steel frames (OMRSF) in accordance with conventional FBD methodology. The optimum designs produced using the CCS algorithm are also compared with those of two metaheuristic search techniques, namely Adaptive Dimensional Search (ADS) (Hasançebi & Kazemzadeh Azad, 2019) and Exponential Big Bang – Big Crunch (EBB-BC) (Hasançebi & Kazemzadeh Azad, 2012), which are deliberately chosen from the literature based on their successful performance reported for this class of problems. Besides, the effect of different search neighborhood schemes ( $nw_c$ ,  $nw_d$ , and  $nw_a$ ) on the performance of CCS algorithm is also scrutinized. These variants of CCS algorithm are denoted as CCS<sub>1</sub>, CCS<sub>2</sub>, and CCS<sub>3</sub>, respectively.

The optimization algorithms are coded in MATLAB R2019a, while structural analysis and design of structural models are carried out via SAP2000 v21.02 through open application programming interface (OAPI). The optimization runs are performed on a PC with Intel i5-6500, 4-core, 3.2 GHz processor, and 16 GB DDR4 Ram operating at 2133 MHz frequency.

The parameter set of ADS, EBB-BC and CCS algorithms used in this study is presented in Table 4.1. Population size ( $\mu$ ) parameter in ADS and EBB-BC algorithms is set to 50 for the first three numerical examples, and 100 for the fourth example. Stagnation control parameters ( $\alpha$  and SEP) used in ADS algorithm for uphill move are taken from Hasançebi & Azad (2015). The termination criterion for

all algorithms is determined as one of the following conditions, whichever is satisfied first: (a) the maximum number of iterations ( $iter^{max}$ ) is reached, (b) if no improvement is achieved during a predefined number of iterations ( $iter^{ni}$ ).

Table 4.1 Algorithm parameters for ADS, EBB-BC, and CCS

<i>Algorithm</i>	<i>Parameters</i>	<i>Stagnation Control</i>	<i>Termination</i>
ADS	$\mu = 50$ (for Example 4, $\mu = 100$ ) $SDR_0 = 0.25$ $SDR_{max} = 0.5$ $SDR_{min} = 1/N_g, \lambda = 0.98$	Uphill move $\alpha = 1.02$ SEP = 20	$iter^{max} = 1000$ $iter^{ni} = 100$
EBB-BC	$\mu = 50$ (for Example 4, $\mu = 100$ ) $\alpha = 1, \lambda = 1$	Not applicable	$iter^{max} = 1000$ $iter^{ni} = 100$
CCS	$\mu = 1$ $P_{min} = 0.02, u = 2, \rho = 3$ $\tau = 0.8$ (for Example 2, $\tau = 0.7$ ) $nW_{min} = 3$ (CCS <sub>3</sub> only)	Uphill move $\alpha = 1.05$ SEP = 30	$iter^{max} = 1000$ $iter^{ni} = 150$

In all design examples, the material properties of the steel are set as follows: modulus of elasticity ( $E$ ) = 29000 ksi (~ 200 GPa), yield strength ( $F_y$ ) = 50 ksi (~ 344.74 MPa), and unit weight ( $\gamma$ ) = 490 lb/ft<sup>3</sup> (~ 76.97 kN/m<sup>3</sup>). In order to size the member groups, a single section pool consisting of 170 AISC standard wide-flange steel sections is used. It should be noted that actually, the complete AISC standard wide-flange steel profile list consists of 297 sections. While forming the section pool, however, some of these sections are eliminated because they are found uneconomical based on their high cross-sectional area and low moment of inertia properties.

The design loads considered for all numerical examples are given in Table 4.2. The earthquake loads are calculated and applied in accordance with the equivalent lateral load procedure in ASCE 7-10. The amplified story drift is limited to 2% of story height. The structural elements are sized in accordance with the provisions of AISC



360-10 design specifications. The design constraints and design load combinations are imposed as described in detail in Chapter 2.

Table 4.2 Design loads and seismic coefficients

Load Type	Example 1 & 2	Example 3 & 4	
		Inner Beams	Outer Beams
Dead Load	24 kN/m	24 kN/m	12 kN/m
Live Load	12 kN/m	12 kN/m	6 kN/m
Seismic Coefficients for BSE-1N			
$S_s$ (g)	$S_1$ (g)	$T_L$ (sec)	Site Class
2.29	0.869	8	D
$F_a$	$F_v$	$S_{DS} = 2/3F_aS_s$	$S_{D1} = 2/3F_vS_1$
1	1.5	1.5267	0.869

#### 4.1.1 Example 1: 28-member planar OMRSF

The first test problem is a planar 4-story, 3-span OMRSF consisting of 28 structural elements grouped into 6 independent sizing variables (Figure 4.1). All structural members are oriented such that their strong axes coincide with the major axis of bending.

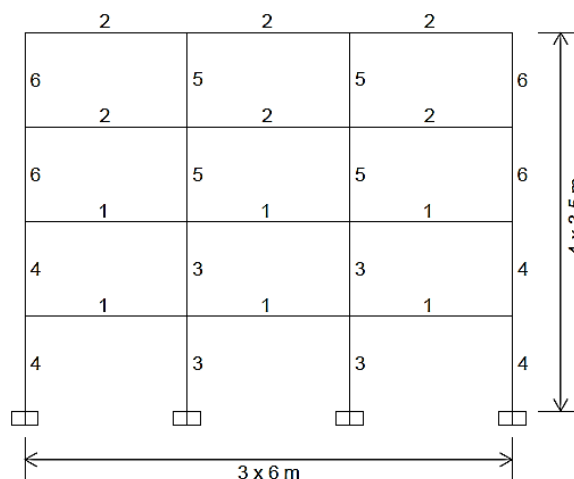


Figure 4.1. 28-member planar OMRSF and grouping of structural elements

Table 4.3 provides a summary of the optimization statistics obtained for this example. It should be noted that since both the CCS and the two metaheuristics employed here are stochastic methods, each optimization algorithm is run 10 times independently to derive statistically meaningful data for a sound comparison of the methods. In Table 4.3, the design weight ( $W$ ) represents the structural weight of the best feasible design obtained during a run under consideration, while the analysis number refers to the total number of structural analyses performed before reaching this optimum solution. Amongst 10 independent runs, the best and the worst runs denote the ones which resulted in minimum and maximum design weights for a steel frame, respectively. In case the minimum weight design is located by multiple runs of an algorithm, the one with the lowest number of structural analyses is recorded as the best run. The best run of each algorithm is highlighted by using **bold font** in the table. The statistical indicators of 10 runs; that is, mean, standard deviation (SD) and coefficient of variation (CV) are also presented in the table for each algorithm. Finally, the computational savings gained through the use of improved upper bound strategy (iUBS) is provided in the last row. This value is simply the ratio of the number of candidate designs rejected without being analyzed to the total number of candidate designs generated throughout the best run.

The results indicate that the minimum design weight of this frame reached in this study is 93.64 kN, and all the algorithms manage to find this solution in one of the ten runs. This solution is presented in Table 4.4 with sectional designations attained for each member group. The number of structural analyses required to obtain this solution appears to be 688 in ADS, 577 in EBB-BC, 326 in CCS<sub>1</sub>, 102 in CCS<sub>2</sub>, and 199 in CCS<sub>3</sub>. It follows that all three variants of the CCS algorithm outperform ADS and EBB-BC metaheuristic techniques in terms of the number of structural analyses performed. The CCS variant with adaptive neighborhood width scheme ( $nw_a$ ), namely CCS<sub>3</sub>, demonstrates the best overall performance as it exhibits the lowest mean (95.32 kN) and coefficient of variation (0.02) among all the algorithms. The variation of the best feasible design throughout the optimization process in the best run of each algorithm is depicted in Figure 4.2.

Table 4.3 Optimization statistics for 28-member planar OMRSF

Algorithm Run #	ADS		EBB-BC		CCS <sub>1</sub>		CCS <sub>2</sub>		CCS <sub>3</sub>	
	W (kN)	# Analyses	W (kN)	# Analyses	W (kN)	# Analyses	W (kN)	# Analyses	W (kN)	# Analyses
1	93.64	4395	118.44	352	98.17	275	<b>93.64</b>	<b>102</b>	97.46	103
2	93.64	2234	96.01	1173	125.60	318	124.82	84	93.64	291
3	<b>93.64</b>	<b>688</b>	95.45	1221	95.72	211	95.73	322	95.11	244
4	117.25	1508	<b>93.64</b>	<b>577</b>	116.50	134	95.62	216	93.64	212
5	94.75	2085	95.20	465	114.11	366	122.69	301	93.64	246
6	93.64	767	95.59	1039	127.49	148	100.49	63	94.06	232
7	95.11	2913	96.84	331	<b>93.64</b>	<b>326</b>	95.62	330	101.03	90
8	95.72	722	98.32	762	98.09	331	93.64	277	<b>93.64</b>	<b>199</b>
9	95.72	863	95.72	718	95.31	284	94.75	280	95.31	282
10	95.72	1002	93.64	801	105.26	192	123.10	104	95.72	210
<b>Mean</b>	96.88	1718	97.88	744	106.99	259	104.01	208	95.32	211
<b>SD</b>	6.84	1151	6.97	305	12.29	78	12.92	102	2.24	64
<b>CV</b>	0.07	0.67	0.07	0.41	0.11	0.30	0.12	0.49	0.02	0.30
<b>iUBS (%)</b>	79.97		88.49		58.20		59.20		49.29	

Table 4.4 Optimum design for 28-member planar OMRSF

Group	Sections
1	W24x55
2	W21x44
3	W24x68
4	W16x45
5	W24x55
6	W14x34
W (kN)	93.64

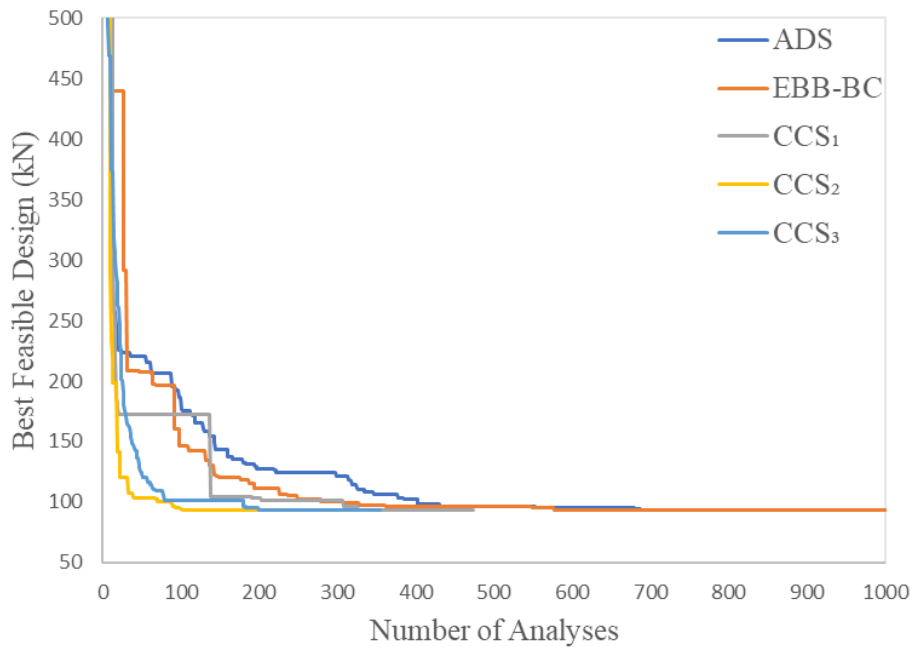


Figure 4.2. Optimization histories for 28-member planar OMRSF

The demand-to-capacity ratios (DCRs) for each member group of the optimum design and inter-story drift ratios in terms of constraint ratios (i.e., max = 1.0) are provided in Table 4.5 and Table 4.6, respectively. It can be concluded that the sectional designations for member groups 2, 3 and 4 are controlled by the corresponding DCR values, which are very close to 1.0. Similarly, the sectional

designations for member groups 5 and 6 are controlled by inter-story drift constraint at the 3<sup>rd</sup> story, which is also very close to 1.0. It should be noted that the elevation level grouping of the members of the frame is implemented separately for every two stories (Figure 4.1). Resultantly, the sectional designations of the drift-controlled members are governed by the greater of the drift ratios in the stories under consideration. It should be underlined that the sectional designations of some member groups might also be controlled by geometric constraints defined for beam-to-column and column-to-column connections. For example, the section depth of the lower floor columns cannot be less than the upper floor columns on the same vertical line, as previously presented in Chapter 2.

Table 4.5 DCRs for 28-member planar OMRSF

<b>Group</b>	<b>DCR</b>
1	0.8863
2	0.9892
3	0.9883
4	0.9884
5	0.7795
6	0.8111
Mean	0.9071
SD	0.0874
CV	0.0964

Table 4.6 Inter-story drift constraints for 28-member planar OMRSF

<b>Story</b>	<b>IDR</b>
1	0.6747
2	0.9324
3	0.9845
4	0.6924
Mean	0.8210
SD	0.1388
CV	0.1691

#### 4.1.2 Example 2: 54-member planar OMRSF

The second test problem is a planar 6-story, 4-span OMRSF consisting of 54 structural elements grouped into 15 independent sizing variables (Figure 4.3). All structural members are oriented such that their strong axes coincide with the major axis of bending.

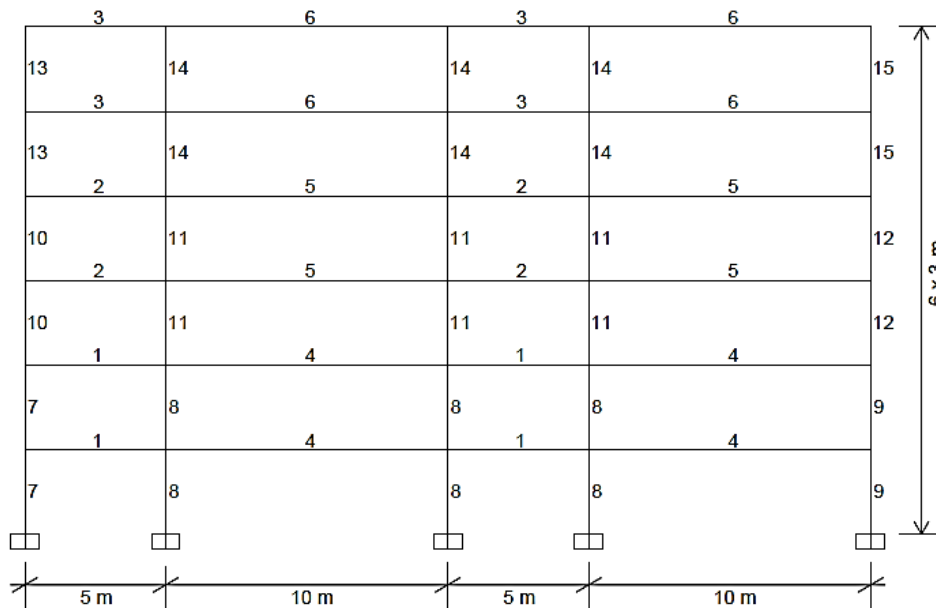


Figure 4.3. 54-member planar OMRSF and grouping of structural elements

For this frame, the results of the independent runs obtained by each optimization method are summarized in Table 4.7 along with statistical evaluations. In Table 4.8, the best feasible design produced for the steel frame in the best run of each algorithm is presented with sectional designations attained for each member group. The variation of the best feasible design throughout the optimization process in the best run of each algorithm is depicted in Figure 4.4.

Table 4.7 Optimization statistics for 54-member planar OMRSF

Algorithm Run #	ADS		EBB-BC		CCS <sub>1</sub>		CCS <sub>2</sub>		CCS <sub>3</sub>	
	W (kN)	# Analyses	W (kN)	# Analyses	W (kN)	# Analyses	W (kN)	# Analyses	W (kN)	# Analyses
1	302.37	1353	298.01	2961	306.87	239	303.12	451	297.21	796
2	295.48	1755	301.96	2371	299.57	611	299.01	483	295.05	435
3	296.12	3853	298.49	4159	302.99	298	297.75	262	299.01	292
4	294.36	1386	300.94	3147	301.54	673	319.83	621	303.18	298
5	<b>293.90</b>	<b>1452</b>	298.38	5705	299.11	362	329.91	228	298.00	320
6	303.58	1652	<b>296.03</b>	<b>3341</b>	308.44	294	<b>293.26</b>	<b>881</b>	299.15	434
7	300.84	1362	304.64	2545	<b>299.01</b>	<b>511</b>	298.44	598	301.09	336
8	296.01	1930	313.96	2225	308.45	298	303.46	253	297.66	275
9	301.54	1803	302.20	3646	301.75	710	765.88	17	<b>293.68</b>	<b>396</b>
10	296.94	1080	296.85	2279	299.96	402	464.08	65	303.16	410
<b>Mean</b>	298.11	1763	301.14	3238	302.77	440	367.47	386	298.72	399
<b>SD</b>	3.40	738	4.97	1019	3.60	165	141.35	256	2.97	144
<b>CV</b>	0.01	0.42	0.02	0.31	0.01	0.37	0.38	0.66	0.01	0.36
<b>iUBS (%)</b>	84.71		91.95		84.89		80.84		84.83	

Similar to previous example, CCS algorithms show superior performance over its metaheuristic counterparts. Considering the best runs of the algorithms, the CCS<sub>2</sub> and CCS<sub>3</sub> provide slightly lighter designs than ADS and EBB-BC algorithms while performing a significantly fewer number of structural analyses. The CCS<sub>3</sub> again provides the most consistent results having the lowest mean (298.72 kN) and coefficient of variation (0.01) amongst all CCS variants. The CCS<sub>3</sub> reaches the optimum solution only after 396 analyses, which is about 88.1% and 72.7% less than EBB-BC (3341 analyses) and ADS (1452 analyses), respectively.

Table 4.8 Optimum designs for 54-member planar OMRSF

<b>Group</b>	<b>ADS</b>	<b>EBB-BC</b>	<b>CCS<sub>1</sub></b>	<b>CCS<sub>2</sub></b>	<b>CCS<sub>3</sub></b>
1	W21x44	W24x68	W16x36	W24x55	W24x55
2	W24x55	W24x55	W21x50	W24x55	W24x55
3	W10x26	W10x26	W10x26	W10x26	W10x26
4	W27x94	W27x84	W27x94	W21x83	W21x83
5	W21x83	W24x84	W27x94	W24x84	W24x84
6	W24x84	W24x84	W24x84	W24x84	W24x84
7	W24x62	W24x84	W24x55	W18x55	W18x60
8	W30x99	W27x94	W30x108	W30x108	W30x108
9	W30x90	W30x90	W30x99	W30x90	W30x90
10	W16x45	W16x45	W16x36	W18x50	W16x50
11	W30x90	W27x84	W30x90	W30x90	W30x90
12	W24x84	W24x84	W30x90	W24x84	W24x84
13	W6x15	W8x24	W6x15	W6x15	W6x15
14	W24x84	W24x84	W24x84	W24x84	W24x84
15	W24x84	W24x84	W24x84	W24x84	W24x84
W (kN)	293.90	296.03	299.01	293.26	293.68
# Analyses	1452	3341	511	881	396



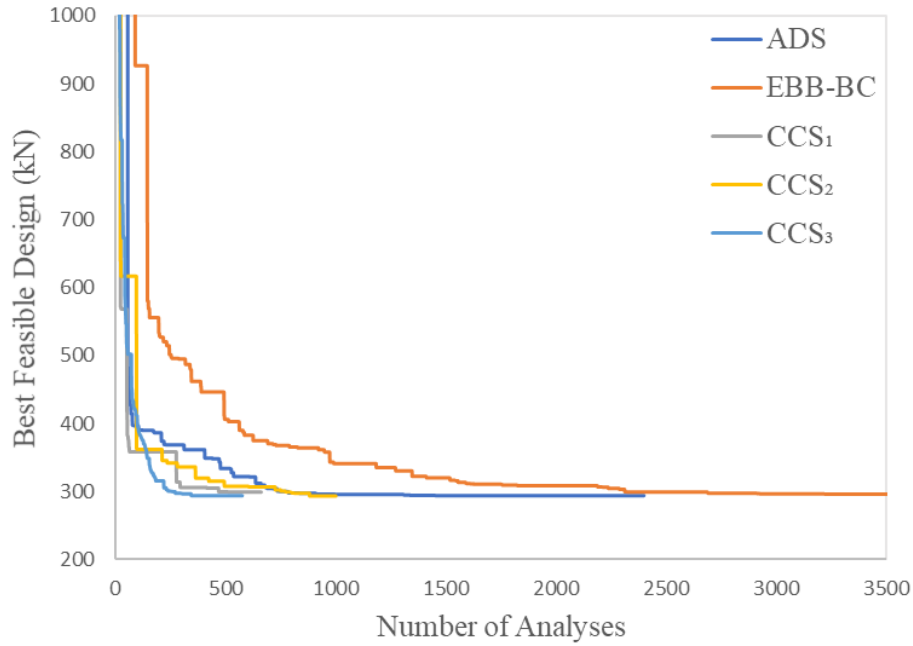


Figure 4.4. Optimization histories for 54-member planar OMRSF

The demand-to-capacity ratios (DCRs) for each member group of the optimum designs produced by each algorithm and inter-story drift ratios in terms of constraint ratios (i.e., max = 1.0) are provided in Table 4.9 and Table 4.10, respectively. It can be concluded that the sectional designations of the member groups with DCRs close to 1.0 are controlled by the corresponding DCR values. On the other hand, the sectional designations of the majority of the remaining member groups are controlled by inter-story drift limitations. It should be remembered that the elevation level grouping of the structural members is implemented separately for every two stories (Figure 4.3). Resultantly, the sectional designations of the drift-controlled members are governed by the greater of the drift ratios in the stories under consideration. As previously elaborated, it should be noted that the sectional designations of some member groups might be controlled by geometric constraints.

Table 4.9 DCRs for 54-member planar OMRSF

<b>Group</b>	<b>ADS</b>	<b>EBB-BC</b>	<b>CCS<sub>1</sub></b>	<b>CCS<sub>2</sub></b>	<b>CCS<sub>3</sub></b>
1	0.8555	0.7096	0.8683	0.9028	0.9014
2	0.8884	0.8112	0.8091	0.8306	0.8341
3	0.9574	0.9217	0.9748	0.9538	0.9543
4	0.9489	0.9968	0.9661	0.9939	0.9974
5	0.9988	0.9812	0.8882	0.9930	0.9958
6	0.9892	0.9960	0.9893	0.9883	0.9884
7	0.9655	0.7942	0.9528	0.9650	0.9072
8	0.9956	0.9998	0.9982	0.9636	0.9604
9	0.9972	0.9796	0.9680	0.9694	0.9677
10	0.8480	0.8717	0.8942	0.7728	0.7968
11	0.7556	0.8611	0.8184	0.7723	0.7760
12	0.6818	0.6681	0.6771	0.6717	0.6722
13	0.9657	0.6591	0.9467	0.9317	0.9406
14	0.5919	0.5808	0.5689	0.5776	0.5776
15	0.4926	0.4983	0.4873	0.4887	0.4888
Mean	0.8621	0.8219	0.8538	0.8517	0.8506
SD	0.1556	0.1598	0.1530	0.1570	0.1545
CV	0.1805	0.1945	0.1791	0.1844	0.1816

Table 4.10 Inter-story drift constraints for 54-member planar OMRSF

<b>Story</b>	<b>ADS</b>	<b>EBB-BC</b>	<b>CCS<sub>1</sub></b>	<b>CCS<sub>2</sub></b>	<b>CCS<sub>3</sub></b>
1	0.5211	0.5165	0.5364	0.5527	0.5499
2	0.8901	0.8474	0.9405	0.9502	0.9474
3	0.9996	0.9763	0.9965	0.9908	0.9935
4	0.9620	0.9203	0.8710	0.8854	0.8894
5	0.9519	0.8995	0.8863	0.9058	0.9053
6	0.6768	0.6622	0.6787	0.6620	0.6624
Mean	0.8336	0.8037	0.8182	0.8245	0.8246
SD	0.1749	0.1618	0.1597	0.1602	0.1613
CV	0.2098	0.2013	0.1952	0.1943	0.1956

### 4.1.3 Example 3: 160-member OMRSF

The third test problem is a 4-story ( $h = 3.5$  m) OMRSF (Figure 4.5a) consisting of 160 structural elements grouped into 12 independent sizing variables. The members are grouped both on plan and elevation levels to satisfy practical fabrication requirements. The plan-level member grouping is performed such that the columns are grouped into four sizing variables as corner columns ( $CG_1$ ), two side columns ( $CG_2, CG_3$ ) inner columns ( $CG_4$ ), and the beams are grouped into two sizing variables as inner beams (IB) and outer beams (OB) (Figure 4.5b). The elevation-level member grouping is carried out such that the structural members have the same sections in every two stories along the height of the frame. Accordingly, there are 4 beam groups and 8 column groups in this example, resulting in 12 independent sizing variables for the entire structure. The orientations of the column groups are displayed in Figure 4.5b, whereas the beams are placed such that their strong axes coincide with the major axis of bending.

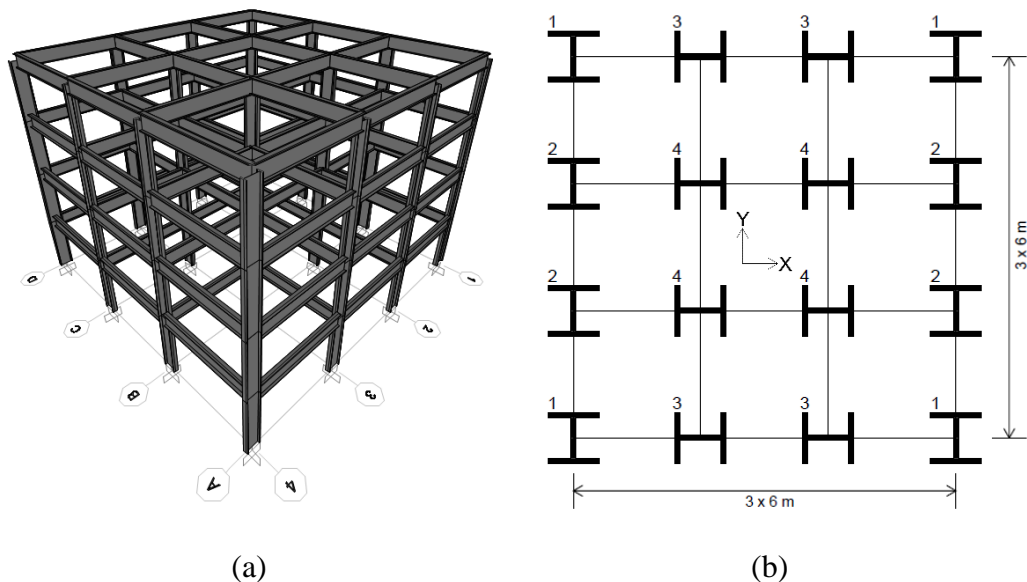


Figure 4.5. 160-member OMRSF, (a) 3D-view (b) plan view

For this frame, the results of the independent runs obtained by each optimization method are summarized in Table 4.11 along with statistical evaluations. In Table 4.12, the best feasible design produced for the steel frame in the best run of each algorithm is presented with sectional designations attained for each member group. The variation of the best feasible design throughout the optimization process in the best run of each algorithm is depicted in Figure 4.6.

In line with the observations in the previous two problems, the superior performance of the CCS algorithms over the two metaheuristics employed is also observed in this example, mainly in terms of convergence rate. Considering the best runs of the algorithms, the CCS<sub>1</sub> and CCS<sub>3</sub> provide slightly lighter designs than ADS and EBB-BC algorithms, yet they require a significantly fewer number of structural analyses to approach the optimum solution. The CCS<sub>3</sub> reaches the optimum solution only after 412 analyses, which is about 74.9% and 90.7% less than EBB-BC (1641 analyses) and ADS (4454 analyses), respectively. Moreover, the CCS<sub>3</sub> provides the most consistent results having the lowest mean (1116.44 kN) and coefficient of variation (0.03) amongst all CCS variants.

The demand-to-capacity ratios (DCRs) for each member group of the optimum designs produced by each algorithm and inter-story drift ratios (for both orthogonal directions) in terms of constraint ratios (i.e., max = 1.0) are provided in Table 4.13, Table 4.14, and Table 4.15, respectively. It can be concluded that the sectional designations of the member groups are mainly controlled by inter-story drift limitations under earthquake loading in y-direction for all of the presented optimum designs. It should be remembered that the elevation level grouping of the structural members is implemented separately for every two stories. Resultantly, the sectional designations of the drift-controlled members are governed by the greater of the drift ratios in the stories under consideration. Again, it should be noted that the sectional designations of some member groups might also be controlled by geometric constraints.

Table 4.11 Optimization statistics for 160-member OMRSF

Algorithm	ADS		EBB-BC		CCS <sub>1</sub>		CCS <sub>2</sub>		CCS <sub>3</sub>	
	W (kN)	# Analyses	W (kN)	# Analyses	W (kN)	# Analyses	W (kN)	# Analyses	W (kN)	# Analyses
1	1089.91	3216	1090.73	2698	1124.00	365	1110.59	318	1122.95	381
2	<b>1078.29</b>	<b>4454</b>	1093.51	3373	1092.68	386	1097.67	440	1129.45	655
3	1110.27	1450	1128.67	4539	<b>1072.45</b>	<b>723</b>	<b>1096.79</b>	<b>790</b>	1107.39	424
4	1182.96	2330	1124.44	2804	1207.91	230	1228.05	244	1158.03	443
5	1089.85	2233	1117.53	2863	1171.54	364	1098.12	178	1178.39	446
6	1184.35	2672	1116.41	3267	1151.35	114	1650.63	645	1112.06	524
7	1274.07	2810	1142.00	3812	1170.84	327	1224.13	431	1088.44	735
8	1090.29	1360	1112.64	2164	1518.58	812	1273.66	269	1105.23	604
9	1133.08	1472	1159.52	2272	1141.18	153	1153.26	428	<b>1059.70</b>	<b>412</b>
10	1113.81	6050	<b>1089.38</b>	<b>1641</b>	1166.21	154	1829.01	145	1102.71	316
<b>Mean</b>	1134.69	2805	1117.48	2943	1181.67	363	1276.19	389	1116.44	494
<b>SD</b>	58.67	1403	21.56	802	118.48	224	242.72	194	31.93	126
<b>CV</b>	0.05	0.50	0.02	0.27	0.10	0.62	0.19	0.50	0.03	0.25
<b>iUBS (%)</b>	73.90		90.39		57.92		44.87		72.37	

Table 4.12 Optimum designs for 160-member OMRSF

Stories	Group	ADS	EBB-BC	CCS <sub>1</sub>	CCS <sub>2</sub>	CCS <sub>3</sub>
1-2	IB	W33x130	W30x90	W33x118	W33x118	W30x108
	OB	W14x30	W24x55	W24x55	W21x50	W24x55
	CG <sub>1</sub>	W40x149	W24x62	W18x60	W14x38	W18x50
	CG <sub>2</sub>	W24x62	W18x60	W18x65	W30x90	W21x62
	CG <sub>3</sub>	W40x221	W36x245	W40x199	W40x249	W40x221
	CG <sub>4</sub>	W40x221	W40x328	W40x268	W40x244	W40x268
3-4	IB	W24x62	W27x84	W21x62	W24x84	W24x68
	OB	W21x50	W18x46	W21x50	W21x50	W21x50
	CG <sub>1</sub>	W30x90	W21x68	W18x50	W14x34	W16x36
	CG <sub>2</sub>	W24x55	W18x46	W18x50	W24x62	W21x50
	CG <sub>3</sub>	W40x221	W30x173	W40x221	W40x192	W30x191
	CG <sub>4</sub>	W40x221	W40x268	W40x244	W40x221	W40x268
W (kN)		1078.29	1089.38	1072.45	1096.79	1059.70
# Analyses		4454	1641	723	790	412

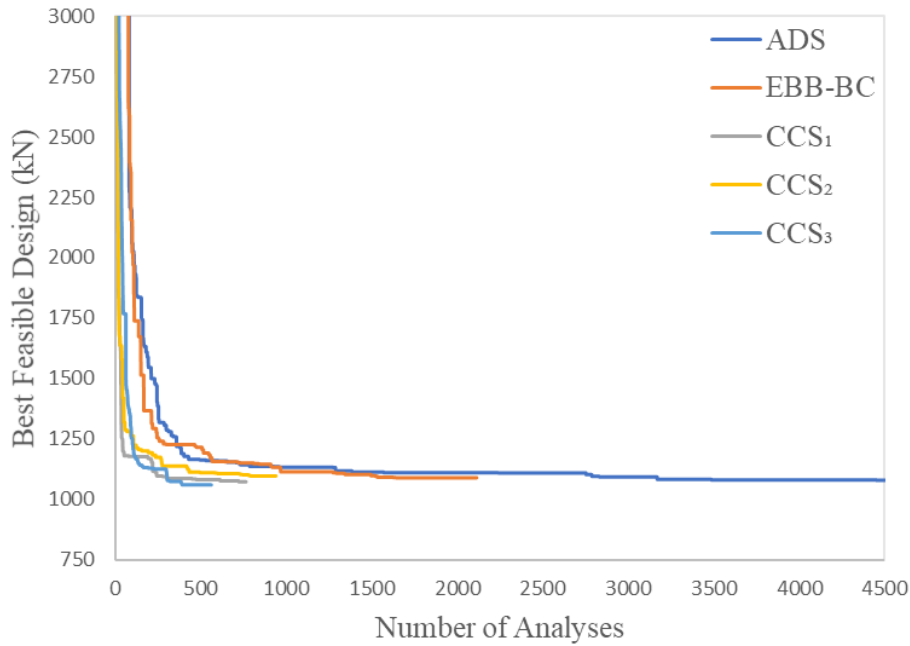


Figure 4.6. Optimization histories for 160-member OMRSF

Table 4.13 DCRs for 160-member OMRSF

Stories	Group	ADS	EBB-BC	CCS <sub>1</sub>	CCS <sub>2</sub>	CCS <sub>3</sub>
1-2	IB	0.6786	0.8056	0.7570	0.7003	0.7911
	OB	0.9691	0.9893	0.9906	0.9713	0.9700
	CG <sub>1</sub>	0.5675	0.9944	0.8567	0.9548	0.9309
	CG <sub>2</sub>	0.9144	0.9527	0.9379	0.8076	0.9691
	CG <sub>3</sub>	0.7315	0.5855	0.6907	0.6430	0.6784
	CG <sub>4</sub>	0.8490	0.6340	0.7510	0.7689	0.7135
3-4	IB	0.9715	0.7454	0.8357	0.7057	0.8213
	OB	0.9929	0.8909	0.9227	0.9870	0.9428
	CG <sub>1</sub>	0.5864	0.5957	0.5921	0.7816	0.7537
	CG <sub>2</sub>	0.7569	0.8795	0.7647	0.7092	0.8642
	CG <sub>3</sub>	0.5043	0.5332	0.5092	0.6092	0.4848
	CG <sub>4</sub>	0.6453	0.5432	0.5679	0.6515	0.5439
Mean		0.7640	0.7625	0.7647	0.7742	0.7886
SD		0.1652	0.1708	0.1469	0.1264	0.1548
CV		0.2162	0.2240	0.1921	0.1633	0.1963

Table 4.14 Inter-story drift constraints for 160-member OMRSF (x-dir.)

Story	ADS	EBB-BC	CCS <sub>1</sub>	CCS <sub>2</sub>	CCS <sub>3</sub>
1	0.4663	0.4219	0.4180	0.4302	0.4455
2	0.9367	0.7996	0.8066	0.8180	0.7913
3	0.9803	0.9757	0.9102	0.9398	0.9236
4	0.8487	0.9059	0.9330	0.8506	0.8521
Mean	0.8080	0.7758	0.7670	0.7597	0.7531
SD	0.2029	0.2137	0.2070	0.1954	0.1837
CV	0.2511	0.2755	0.2699	0.2572	0.2439

Table 4.15 Inter-story drift constraints for 160-member OMRSF (y-dir.)

Story	ADS	EBB-BC	CCS <sub>1</sub>	CCS <sub>2</sub>	CCS <sub>3</sub>
1	0.9049	0.8217	0.8936	0.8873	0.8613
2	0.9937	0.9921	0.9764	0.9745	0.9898
3	0.9933	0.9965	0.9896	0.9949	0.9983
4	0.7878	0.7666	0.8164	0.6887	0.7126
Mean	0.9199	0.8942	0.9190	0.8864	0.8905
SD	0.0844	0.1020	0.0697	0.1210	0.1162
CV	0.0917	0.1140	0.0759	0.1366	0.1305

#### 4.1.4 Example 4: 584-member OMRSF

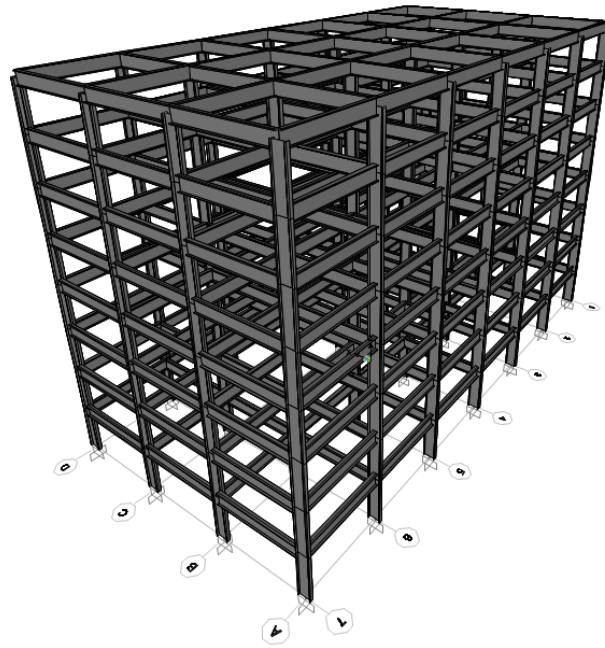
The fourth test problem is an 8-story ( $h = 3$  m) space OMRSF (Figure 4.7a) consisting of 584 structural elements grouped into 24 independent sizing variables. The members are grouped both on plan and elevation levels to satisfy practical fabrication requirements. The plan-level member grouping is performed such that the columns are grouped into four sizing variables as corner columns ( $CG_1$ ), two side columns ( $CG_2, CG_3$ ) inner columns ( $CG_4$ ), and the beams are grouped into two sizing variables as inner beams (IB) and outer beams (OC) (Figure 4.7b). The elevation-level member grouping is carried out such that the structural members have the same sections in every two stories along the height of the frame. Accordingly, there are 8 beam groups and 16 column groups in this example, resulting in 24 independent sizing variables for the entire structure. The orientations of the column groups are displayed in Figure 4.7b, whereas the beams are placed such that their strong axes coincide with the major axis of bending.

For this frame, the results of the independent runs obtained by each optimization method are summarized in Table 4.16 along with statistical evaluations. In Table 4.17, the best feasible design produced for the steel frame in the best run of each algorithm is presented with sectional designations attained for each member group. The variation of the best feasible design throughout the optimization process in the best run of each algorithm is depicted in Figure 4.8.

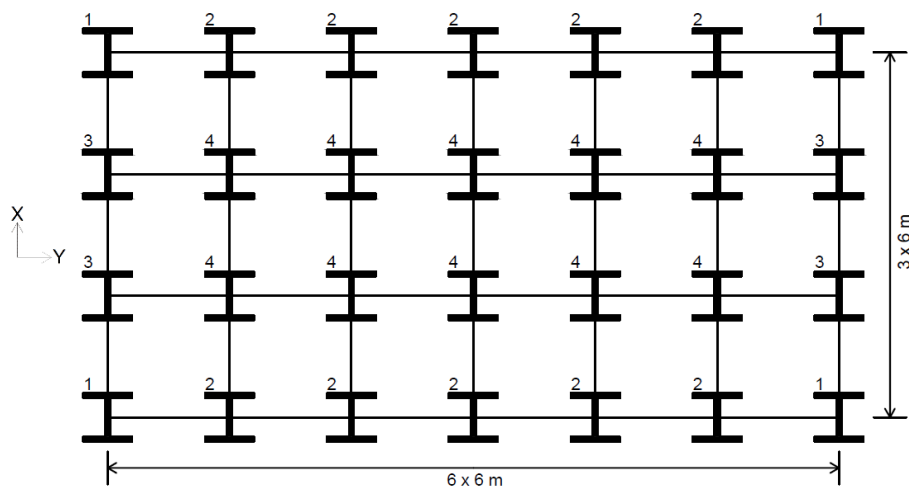
Unlike previous examples, none of the CCS variants manage to reach a better solution than its metaheuristic counterparts. The optimum design obtained by the most successful variant of CCS in this example,  $CCS_3$ , is 4878.14 kN, which is 182.31 kN (3.88%) heavier than the optimum design obtained by ADS (4695.83 kN), and only 0.79 kN (0.016 %) heavier than the optimum design found by EBB-BC (4877.35 kN). On the other hand, the  $CCS_3$  reaches the optimum solution with significantly less computational effort; namely only after 875 analyses, which is about 70.2% and 83.9% less than EBB-BC (2935 analyses) and ADS (5462 analyses), respectively. When the mean design weights are compared, it is seen that



the CCS<sub>3</sub> (5027.66 kN) is 6.3% lighter than EBB-BC (5363.18 kN) and is only slightly heavier (0.2%) than the ADS (5017.51 kN).



(a)



(b)

Figure 4.7. 584-member OMRSF, (a) 3D-view (b) plan view

Table 4.16 Optimization statistics for 584-member OMRSF

Algorithm Run #	ADS		EBB-BC		CCS <sub>1</sub>		CCS <sub>2</sub>		CCS <sub>3</sub>	
	W (kN)	# Analyses	W (kN)	# Analyses	W (kN)	# Analyses	W (kN)	# Analyses	W (kN)	# Analyses
1	4926.87	4262	5623.32	2482	5527.33	222	5714.79	375	4965.13	833
2	4904.35	5294	5348.54	2162	6820.58	69	5390.50	501	5096.05	474
3	4850.00	5361	5604.25	2340	5231.33	464	<b>5045.76</b>	<b>746</b>	5042.06	757
4	4797.80	4367	5172.15	2279	5601.15	97	5437.04	356	<b>4878.14</b>	<b>875</b>
5	<b>4695.83</b>	<b>5462</b>	5235.02	3041	5379.05	367	5045.58	866	5070.14	952
6	4709.11	3351	5132.40	3287	5582.38	282	5149.20	811	5104.04	790
7	5658.96	2498	5467.67	2776	5275.84	725	5485.90	184	4943.97	992
8	5439.00	8912	5397.75	2377	<b>5197.90</b>	<b>453</b>	5143.96	422	4974.66	650
9	5318.75	4182	<b>4877.35</b>	<b>2935</b>	5576.90	251	5205.40	336	4987.71	634
10	4874.43	3806	5773.31	1168	5305.94	661	5185.50	561	5214.64	426
<b>Mean</b>	5017.51	4750	5363.18	2485	5549.84	359	5280.36	516	5027.66	738
<b>SD</b>	315.64	1647	254.66	562	448.19	208	206.94	215	92.28	181
<b>CV</b>	0.06	0.35	0.05	0.23	0.08	0.58	0.04	0.42	0.02	0.24
<b>iUBS (%)</b>	83.10		97.06		89.50		85.87		93.11	

Table 4.17 Optimum designs for 584-member OMRSF

Stories	Group	ADS	EBBBC	UUSS <sub>1</sub>	UUSS <sub>2</sub>	UUSS <sub>3</sub>
1-2	IB	W33x130	W33x130	W36x135	W30x116	W33x118
	OB	W30x90	W24x68	W24x76	W24x68	W24x62
	CG <sub>1</sub>	W33x118	W40x149	W40x149	W44x248	W36x210
	CG <sub>2</sub>	W40x192	W40x298	W40x268	W40x268	W40x298
	CG <sub>3</sub>	W36x160	W44x248	W40x268	W40x324	W40x298
	CG <sub>4</sub>	W40x328	W40x328	W40x362	W40x328	W40x397
3-4	IB	W30x116	W30x108	W30x116	W27x114	W30x99
	OB	W24x84	W27x84	W24x76	W24x68	W24x68
	CG <sub>1</sub>	W24x104	W27x84	W30x191	W30x173	W27x161
	CG <sub>2</sub>	W40x192	W40x268	W40x221	W40x244	W40x268
	CG <sub>3</sub>	W30x191	W36x245	W36x527	W40x268	W33x263
	CG <sub>4</sub>	W40x298	W40x298	W36x280	W33x387	W40x328
5-6	IB	W30x90	W30x90	W30x90	W30x90	W30x90
	OB	W24x62	W24x55	W24x76	W24x68	W24x55
	CG <sub>1</sub>	W24x104	W18x60	W24x94	W27x94	W24x104
	CG <sub>2</sub>	W40x192	W40x221	W36x245	W36x230	W40x221
	CG <sub>3</sub>	W27x161	W33x201	W40x192	W30x173	W30x191
	CG <sub>4</sub>	W40x268	W40x268	W30x357	W33x387	W40x298
7-8	IB	W21x50	W18x55	W21x57	W24x62	W24x55
	OB	W21x50	W18x40	W18x35	W18x40	W21x44
	CG <sub>1</sub>	W24x104	W18x60	W24x104	W24x104	W10x33
	CG <sub>2</sub>	W24x131	W40x199	W27x146	W27x146	W30x173
	CG <sub>3</sub>	W24x117	W24x103	W21x68	W30x116	W27x258
	CG <sub>4</sub>	W40x221	W40x268	W30x326	W36x230	W33x201
W (kN)		4695.83	4877.35	5197.90	5045.58	4878.14
# Analyses		5462	2935	454	746	875

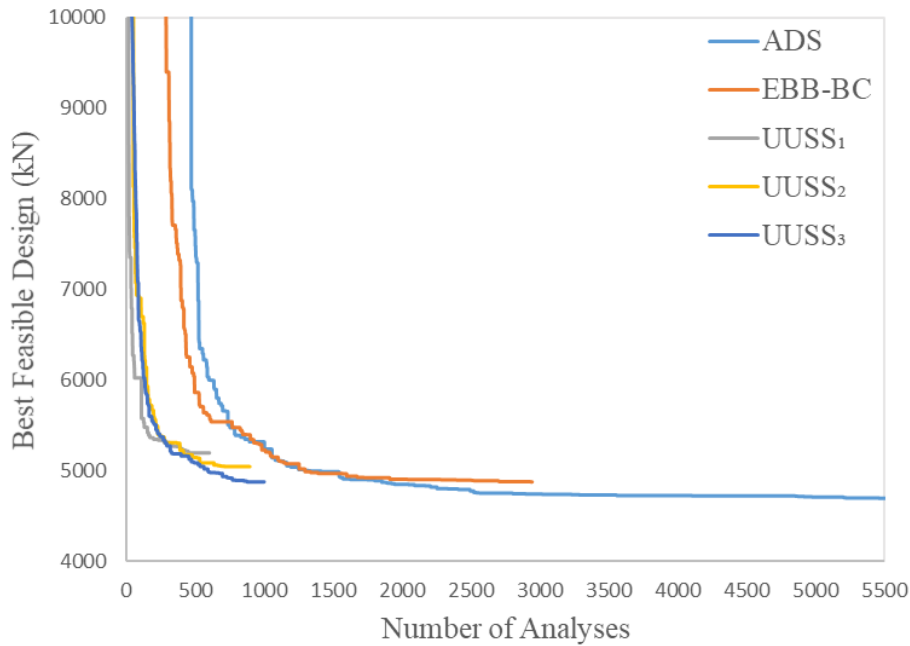


Figure 4.8. Optimization histories for 584-member OMRSF

The demand-to-capacity ratios (DCRs) for each member group of the optimum designs produced by each algorithm and inter-story drift ratios (for both orthogonal directions) in terms of constraint ratios (i.e., max = 1.0) are provided in Table 4.18, Table 4.19, and Table 4.20, respectively. Similar to the previous example, the sectional designations of the member groups are mainly controlled by inter-story drift limitations under earthquake loading in y-direction for all of the presented optimum designs. It should be remembered that the elevation level grouping of the structural members is implemented separately for every two stories. Resultantly, the sectional designations of the drift-controlled members are governed by the greater of the drift ratios in the stories under consideration. It should be emphasized that the sectional designations of some member groups might be controlled by geometric constraints, as previously discussed.

Table 4.18 DCRs for 584-member OMRSF

Stories	Group	ADS	EBB-BC	CCS <sub>1</sub>	CCS <sub>2</sub>	CCS <sub>3</sub>
1-2	IB	0.5543	0.5657	0.5380	0.6237	0.5851
	OB	0.4940	0.6220	0.5571	0.5659	0.7643
	CG <sub>1</sub>	0.8144	0.6546	0.6767	0.4435	0.4634
	CG <sub>2</sub>	0.9174	0.5571	0.6001	0.5990	0.5372
	CG <sub>3</sub>	0.9274	0.7396	0.8311	0.6814	0.7438
	CG <sub>4</sub>	0.8654	0.8424	0.7732	0.8032	0.7072
3-4	IB	0.6373	0.6810	0.6682	0.6600	0.7030
	OB	0.5591	0.5927	0.5941	0.6273	0.6593
	CG <sub>1</sub>	0.7848	0.7926	0.4949	0.4945	0.4925
	CG <sub>2</sub>	0.7663	0.5258	0.5694	0.4966	0.4549
	CG <sub>3</sub>	0.7881	0.6637	0.3992	0.5510	0.5498
	CG <sub>4</sub>	0.7541	0.7389	0.7986	0.5908	0.6692
5-6	IB	0.6837	0.7072	0.6911	0.6958	0.6926
	OB	0.7354	0.8850	0.5556	0.5864	0.9031
	CG <sub>1</sub>	0.5981	0.7268	0.5426	0.6167	0.5792
	CG <sub>2</sub>	0.6211	0.5716	0.4772	0.5030	0.4864
	CG <sub>3</sub>	0.6372	0.5786	0.6643	0.6002	0.5919
	CG <sub>4</sub>	0.6600	0.6493	0.5779	0.4942	0.5926
7-8	IB	0.9251	0.7445	0.8183	0.7258	0.8578
	OB	0.6156	0.8089	0.9843	0.7183	0.8902
	CG <sub>1</sub>	0.5151	0.5696	0.5477	0.5425	0.6832
	CG <sub>2</sub>	0.5365	0.4006	0.5042	0.4861	0.4420
	CG <sub>3</sub>	0.5798	0.5622	0.6437	0.6081	0.4119
	CG <sub>4</sub>	0.5642	0.4895	0.4408	0.5582	0.5654
Mean		0.6889	0.6529	0.6228	0.5947	0.6261
SD		0.1325	0.1157	0.1364	0.0867	0.1374
CV		0.1924	0.1772	0.2190	0.1457	0.2194

Table 4.19 Inter-story drift constraints for 584-member OMRSF (x-dir.)

<b>Story</b>	<b>ADS</b>	<b>EBB-BC</b>	<b>CCS<sub>1</sub></b>	<b>CCS<sub>2</sub></b>	<b>CCS<sub>3</sub></b>
1	0.2898	0.2671	0.2746	0.3006	0.2582
2	0.5256	0.5301	0.5575	0.5726	0.5467
3	0.6546	0.6544	0.6401	0.6888	0.7115
4	0.7134	0.6885	0.6899	0.7220	0.7575
5	0.7583	0.7607	0.6971	0.7415	0.8162
6	0.7303	0.7915	0.6823	0.6717	0.7798
7	0.7412	0.8482	0.8079	0.6668	0.7713
8	0.7092	0.7042	0.7652	0.6111	0.6397
Mean	0.6403	0.6556	0.6393	0.6219	0.6601
SD	0.1494	0.1720	0.1548	0.1319	0.1725
CV	0.2333	0.2624	0.2421	0.2120	0.2613

Table 4.20 Inter-story drift constraints for 584-member OMRSF (y-dir.)

<b>Story</b>	<b>ADS</b>	<b>EBB-BC</b>	<b>CCS<sub>1</sub></b>	<b>CCS<sub>2</sub></b>	<b>CCS<sub>3</sub></b>
1	0.8523	0.8102	0.7885	0.7760	0.7559
2	0.9975	0.9768	0.9707	0.9912	0.9986
3	0.9971	0.9831	0.9832	0.9989	0.9958
4	0.9930	0.9774	0.9878	0.9692	0.9895
5	0.9970	0.9951	0.9839	0.9918	0.9824
6	0.8794	0.9736	0.8567	0.8215	0.8752
7	0.9971	0.9941	0.9918	0.9932	0.9773
8	0.7689	0.7979	0.7736	0.6997	0.7112
Mean	0.9353	0.9385	0.9170	0.9052	0.9107
SD	0.0839	0.0780	0.0888	0.1126	0.1094
CV	0.0897	0.0832	0.0968	0.1244	0.1202

## 4.2 Summary

The results of all four example problems presented in this chapter indicate that the  $CCS_3$ , which utilizes adaptive search neighborhood width ( $nw_a$ ), is the most efficient CCS variant in terms of the quality of the optimum solution obtained, consistency of the results, and the convergence rate.

It is also shown that the proposed CCS algorithm, can successfully be applied to sizing optimization problems of steel frame structures with displacement constraints, and it provides substantial computational savings (~65-90%) while producing optimum designs comparable to the metaheuristics, if not the better.

It should also be noted that the number of structural analyses required for ADS, EBB-BC, and CCS for the presented examples are reduced significantly through implementation of iUBS (~45-95%). The effect of iUBS is much more pronounced for complex structural models as there are more connections and equally increased number of geometrical constraints. Therefore, a higher number of candidate designs are eliminated without being analyzed when iUBS rather than UBS is employed, because the former considers not only the weight but also geometrical constraints for pre-analysis evaluation of a candidate design, while the latter considers only the weight, as explained before.





## CHAPTER 5

### PERFORMANCE BASED DESIGN OPTIMIZATION

In this chapter, the numerical examples are presented for performance-based design optimization of steel frames. The steel frames that were introduced in the previous chapter are again sized for minimum weight; albeit using PDB methodology this time. The CCS algorithm, which is proposed and evaluated in the previous chapters, is used for the optimization of these frames. The study also aims to carry out a comparison between optimally designed structures under conventional force-based design and performance-based design approaches in terms of cost and seismic performance.

#### 5.1 Performance Based Design using SAP2000 OAPI

In the current version of SAP2000v21.02, there is no OAPI function to retrieve plastic hinge deformations and acceptance criteria for varying performance levels. On the other hand, these data are required and essential for the CCS algorithm since the optimization process is guided by this algorithm based on the evaluation of DCRs. A workaround to this problem is to export all the required data to MS Excel by using the database tables feature of SAP2000. After that, one can import this data from the excel file to any computing platform (such as MATLAB in this study) and calculate the corresponding DCRs for each design group. The optimization process can then proceed as projected. Nevertheless, the exporting and importing sequences are computationally intensive tasks which can take a significant amount of time especially for structural models with a large number of hinges. It should also be noted that the number of saved states during analysis directly affects the time of export from SAP2000 and processing time of imported data in MATLAB. Decreasing the

number of saved states, on the other hand, may result in missing the optimum designs in between two consecutive pushover steps, if any.

## 5.2 Numerical Examples

The same steel design examples (1-3) from the previous chapter are used for the performance-based design optimization studies. The basic performance objective equivalent to new building standards (BPON) given in ASCE 41-13 guidelines is adopted. BPON foresees a Life Safety (LS) structural performance level and Position Retention non-structural performance level under BSE-1N hazard level; and Collapse Prevention (CP) structural performance level under BSE-2N hazard level while non-structural performance is not considered. BSE-2N corresponds to Targeted Maximum Considered Earthquake ( $MCE_R$ ) and can be thought of as a seismic hazard with 2% probability of exceedance in 50 years. (2%/50-year). BSE-1N, on the other hand, corresponds to design earthquake level and can be taken as  $2/3$  of  $MCE_R$  (ASCE 41-13).

In order to evaluate seismic performance of the steel frames, pushover analysis with a lateral load pattern reflecting the fundamental mode shape in the direction under consideration is used. In all the examples, the structures are pushed under this load pattern until the roof displacement reaches 5% of the building height. The number of saved states is set to 100 for the first two examples, and to 50 for the third example. The determination of the target displacement for pushover analysis is performed in accordance with ASCE 41-13 requirements. The plastic hinges are defined at the start and the end node of each structural element. Modeling parameters and acceptance criteria of the hinges are also determined in accordance with ASCE 41-13.

At the target displacements corresponding to BSE-1N and BSE-2N hazard levels, plastic hinge rotation constraints of the deformation-controlled members and strength constraints of the force-controlled members are considered for the

performance-based design. In addition, at BSE-1N hazard level, an inter-story drift limit of 2% of the story height is considered for each story in accordance with BPON requirements for the position retention non-structural performance level. Gravity loads and seismic coefficients are taken as given for the conventional force-based design in Chapter 4, Table 4.2. All details related to design constraints and load combinations are taken as previously presented in Chapter 2.

For all three examples, the CCS<sub>3</sub> algorithm is employed, in which the only change to default algorithm parameters given in Table 4.1 is made for  $\tau$  such that it is taken as 0.8 for the first example and 0.7 for the second and third examples. For all the examples, SEP and  $iter^{ni}$  parameters are taken as 50 and 150, respectively. The maximum number of iterations parameter,  $iter^{max}$ , is set to 500 for the first and third examples, and to 1000 for the second example. Ten independent optimization runs are performed for each example while the initial design is defined by assigning the largest available sections for each member group. The best run results are presented and used for comparison with the optimum designs produced according to FBD approach in the previous chapter in terms of cost and seismic performance.

### **5.2.1 Example 1: 28-member planar OMRSF**

Table 5.1 presents and compares the optimum designs of the 28-member planar OMRSF produced according to PBD and FBD methodologies. Table 5.2 shows the number of structural elements satisfying various performance levels under BSE-1N and BSE 2-N hazard levels in accordance with the BPON. In addition, the maximum inter-story drift ratios for both designs at the corresponding target displacements are also provided in the table. It should be noted that although the pushover load is applied in one direction (+x) only, while Table 5.2 is being formed, the effect of the loading in the (-x) direction is also considered by taking advantage of the symmetrical plan and member grouping of the structural model. The results show that the optimum design of the frame produced according to PBD methodology is 5.64% lighter than the one produced according to FBD methodology. While the

former complies with all BPON requirements, the latter fails to satisfy BPON requirements since it has two structural members deforming beyond CP level at BSE-1N and BSE-2N hazard levels.

Table 5.1 Optimum PBD and FBD for Example 1

Group	PBD	FBD
1	W21x50	W24x55
2	W18x40	W21x44
3	W21x83	W24x68
4	W12x35	W16x45
5	W21x57	W24x55
6	W12x26	W14x34
W (kN)	88.36	93.64
# Analysis	215	199

Table 5.2 Comparison of optimum PBD and FBD for Example 1.

Hazard	BSE-1N		BSE-2N	
Design P. Level	PBD	FBD	PBD	FBD
IO	22	24	12	21
LS	6	2	16	5
CP	0	0	0	0
> CP	0	2	0	2
IDR <sub>max</sub> (%)	2.00	1.75	-	-

The hinge states at the target displacements corresponding to BSE-2N hazard level for optimum PBD and FBD are also illustrated in Figure 5.1. It is apparent that the optimum PBD yields in more homogeneous distribution of the inelastic deformation demands over the entire structure than does the optimum FBD. The pushover capacity curves for both designs are depicted in Figure 5.2. The variation of the best feasible design throughout the optimization process with PBD methodology is shown in Figure 5.3.

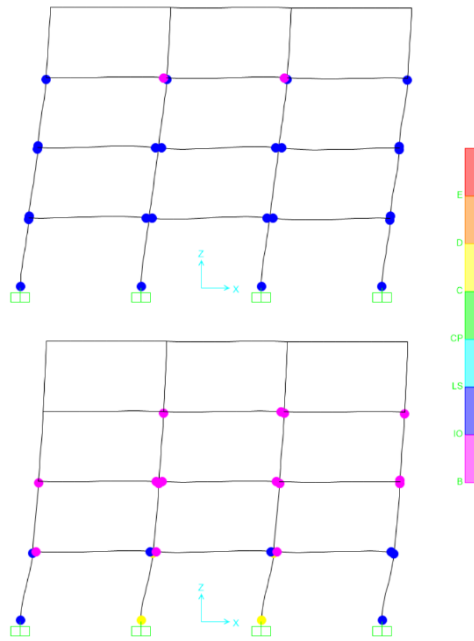


Figure 5.1. Hinge states (BSE-2N) for optimum PBD (top) and FBD (bottom) for Example 1

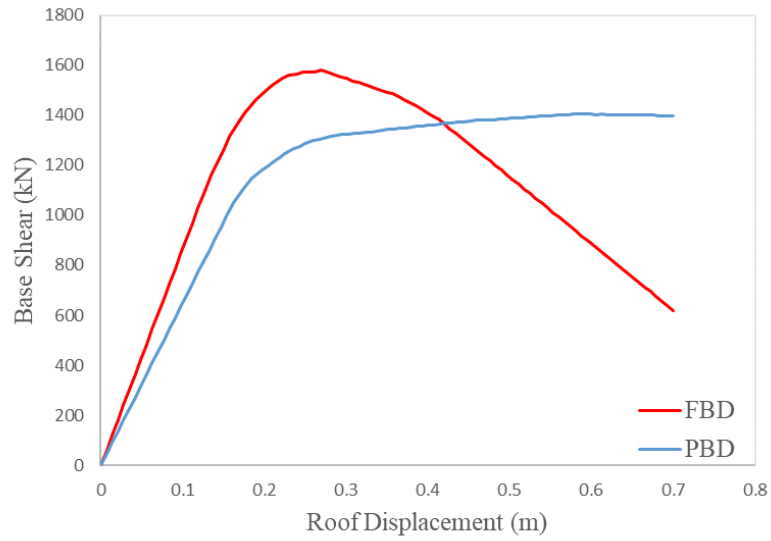


Figure 5.2. Pushover capacity curves of optimum PBD and FBD for Example 1

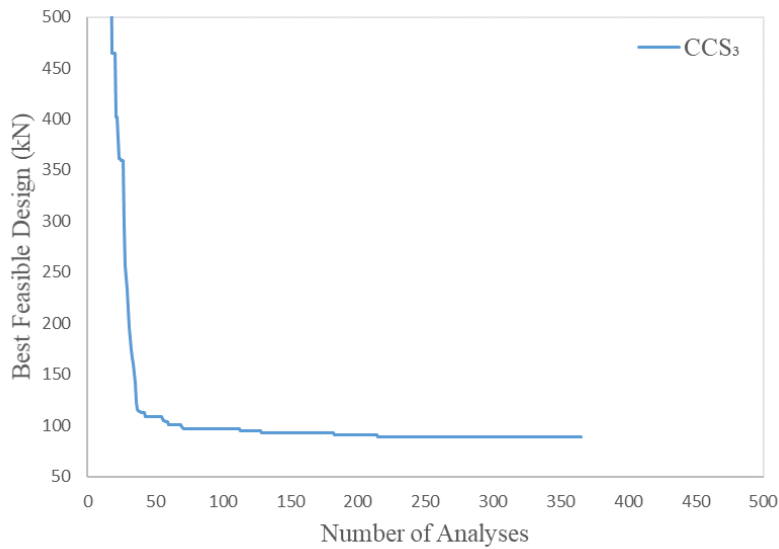


Figure 5.3. Optimization history for Example 1 (PBD)

### 5.2.2 Example 2: 54-member planar OMRSF

Table 5.3 presents and compares the optimum designs of the 54-member planar OMRSF produced according to PBD and FBD methodologies. Since the structural plan of the frame is asymmetric, two cases of pushover analysis are considered in which the lateral load pattern is applied in opposite directions. Table 5.4 shows the number of structural elements satisfying various performance levels under BSE-1N and BSE 2-N hazard levels in accordance with the BPON. In addition, the maximum inter-story drift ratios for both designs at the corresponding target displacements are also provided in the table. The results show that the optimum design of the frame produced according to PBD methodology is 1.43% lighter than the one produced according to FBD methodology. While the former complies with all BPON requirements, the latter fails to satisfy BPON requirements since it has multiple members deforming beyond CP level at BSE-1N and BSE-2N hazard levels.

The hinge states at the target displacements corresponding to BSE-2N hazard level for optimum PBD and FBD are also illustrated in Figure 5.4-5.5. Similar to previous

example, it can be observed that the optimum PBD results in more homogeneous distribution of the inelastic deformation demands over the entire structure than does the optimum FBD. The pushover capacity curves for both designs are depicted in Figure 5.6. The variation of the best feasible design throughout the optimization process with PBD methodology is shown in Figure 5.7.

Table 5.3 Optimum PBD and FBD for Example 2

Group	PBD	FBD
1	W16x26	W24x55
2	W16x26	W24x55
3	W10x26	W10x26
4	W30x90	W21x83
5	W27x84	W24x84
6	W24x84	W24x84
7	W16x40	W18x60
8	W40x149	W30x108
9	W30x90	W30x90
10	W16x31	W16x50
11	W30x90	W30x90
12	W30x90	W24x84
13	W6x20	W6x15
14	W24x84	W24x84
15	W24x84	W24x84
W (kN)	289.48	293.68
# Analysis	220	396

Table 5.4 Comparison of optimum PBD and FBD for Example 2

Hazard Design P. Level	BSE-1N		BSE-2N	
	PBD	FBD	PBD	FBD
IO	40	44	30	35
LS	14	7	21	15
CP	0	0	3	0
> CP	0	3	0	4
IDR <sub>max</sub> (%)	2.00	1.95	-	-

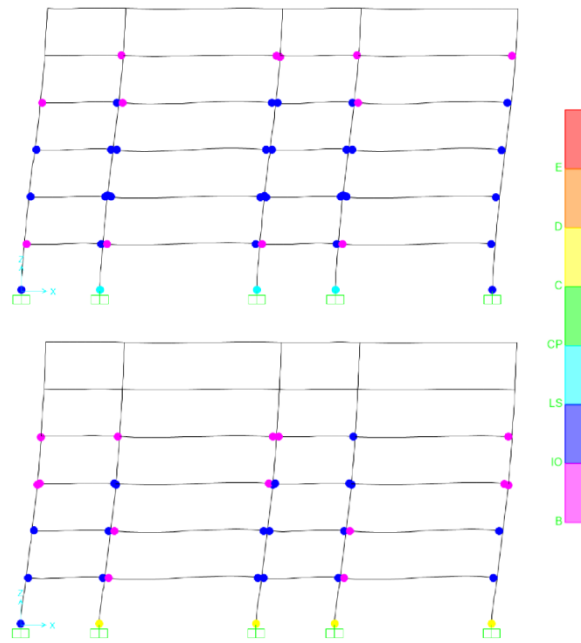


Figure 5.4. Hinge states (BSE-2N) for optimum PBD (top) and FBD (bottom) for Example 2 (+x loading)

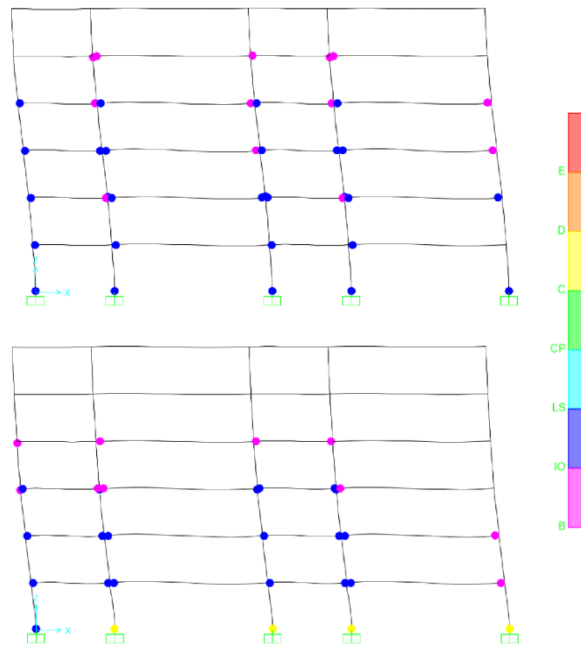


Figure 5.5. Hinge states (BSE-2N) for optimum PBD (top) and FBD (bottom) for Example 2 (-x loading)



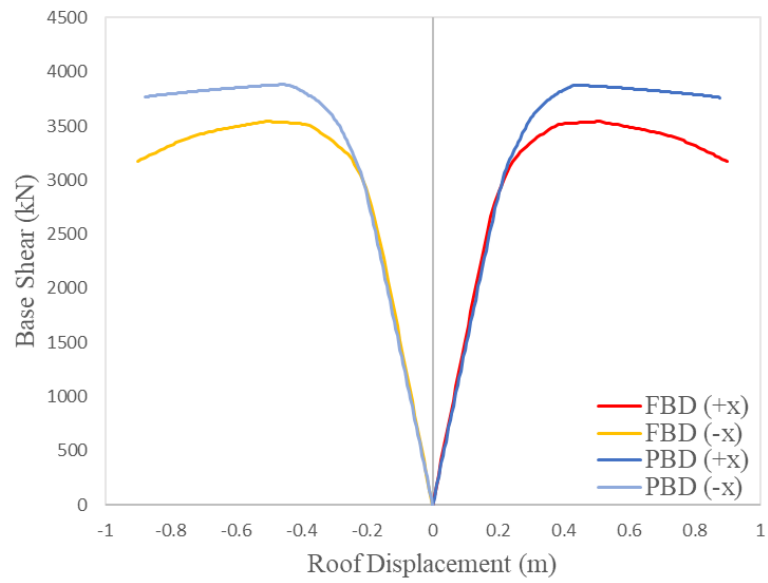


Figure 5.6. Pushover capacity curves of optimum PBD and FBD for Example 2

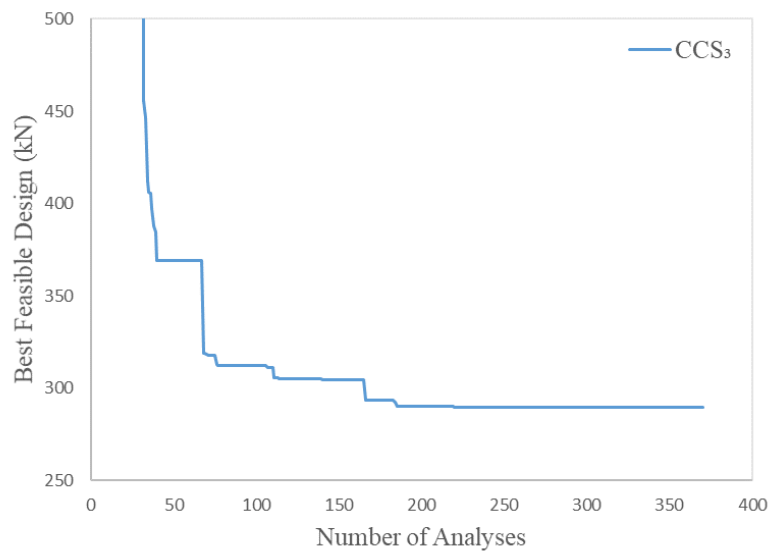


Figure 5.7. Optimization history for Example 2 (PBD)

### 5.2.3 Example 3: 160-member OMRSF

Table 5.5 presents and compares the optimum designs of the 160-member OMRSF (Example 3) produced according to PBD and FBD methodologies. Since the structural plan and grouping of structural elements are symmetrical about both lateral directions, two cases of pushover analysis are considered only in which the lateral load pattern is applied in either (+x) or (+y) direction. Table 5.6 shows the number of structural elements satisfying various performance levels under BSE-1N and BSE 2-N hazard levels in accordance with the BPON. In addition, the maximum inter-story drift ratios for both designs at the corresponding target displacements are also provided in the table. It should be noted that although the pushover load is applied only in (+x) and (+y) directions, while Table 5.6 is being formed, the effect of the loading in the reverse directions are also considered by taking advantage of the symmetrical plan and member grouping of the structural model.

Table 5.5 Optimum PBD and FBD for Example 3

Stories	Group	PBD	FBD
1-2	IB	W24x84	W30x108
	OB	W24x55	W24x55
	CG <sub>1</sub>	W21x62	W18x50
	CG <sub>2</sub>	W30x116	W21x62
	CG <sub>3</sub>	W40x215	W40x221
	CG <sub>4</sub>	W36x300	W40x268
3-4	IB	W24x84	W24x68
	OB	W18x35	W21x50
	CG <sub>1</sub>	W18x35	W16x36
	CG <sub>2</sub>	W18x46	W21x50
	CG <sub>3</sub>	W40x192	W30x191
	CG <sub>4</sub>	W33x201	W40x268
W (kN)		1020.39	1059.70
# Analysis		405	412

Table 5.6 Comparison of optimum PBD and FBD for Example 3

<b>Hazard</b>	<b>BSE-1N</b>		<b>BSE-2N</b>	
<b>Design</b> <b>P. Level</b>	<b>PBD</b>	<b>FBD</b>	<b>PBD</b>	<b>FBD</b>
IO	144	146	102	108
LS	16	14	58	44
CP	0	0	0	4
> CP	0	0	0	4
<b>IDR<sub>max</sub> (%)</b>	2.00	2.77	-	-

The results show that the optimum design of the frame produced according to FBD fails to meet BPON requirements as inter-story drift constraints are violated at BSE-1N hazard level; and four structural elements deform beyond collapse prevention level in BSE-2N hazard. On the other hand, the optimum design of the frame produced according to PBD methodology, while satisfying all BPON requirements, is 3.71% lighter than its FBD counterpart.

The hinge states at the target displacements corresponding to BSE-2N hazard level for optimum PBD and FBD are also illustrated in Figure 5.8-5.9. It can be concluded that the optimum PBD results in more homogeneous distribution of the inelastic deformation demands over the entire structure than does the optimum FBD.

The pushover capacity curves for both designs are depicted in Figure 5.10. The variation of the best feasible design throughout the optimization process with PBD methodology is shown in Figure 5.11.

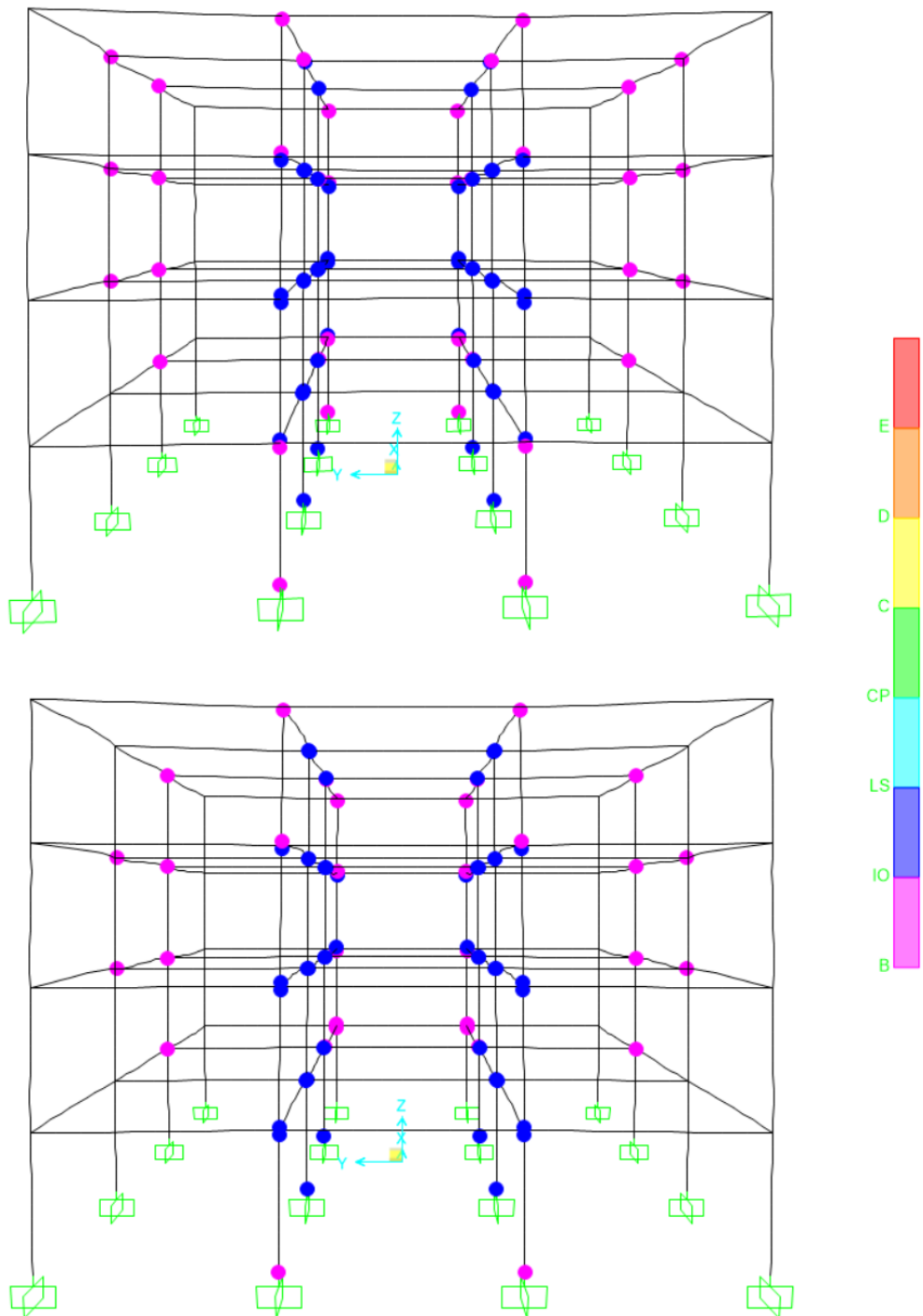


Figure 5.8. Hinge states (BSE-2N) for optimum PBD (top) and FBD (bottom) for Example 3 (+x loading)

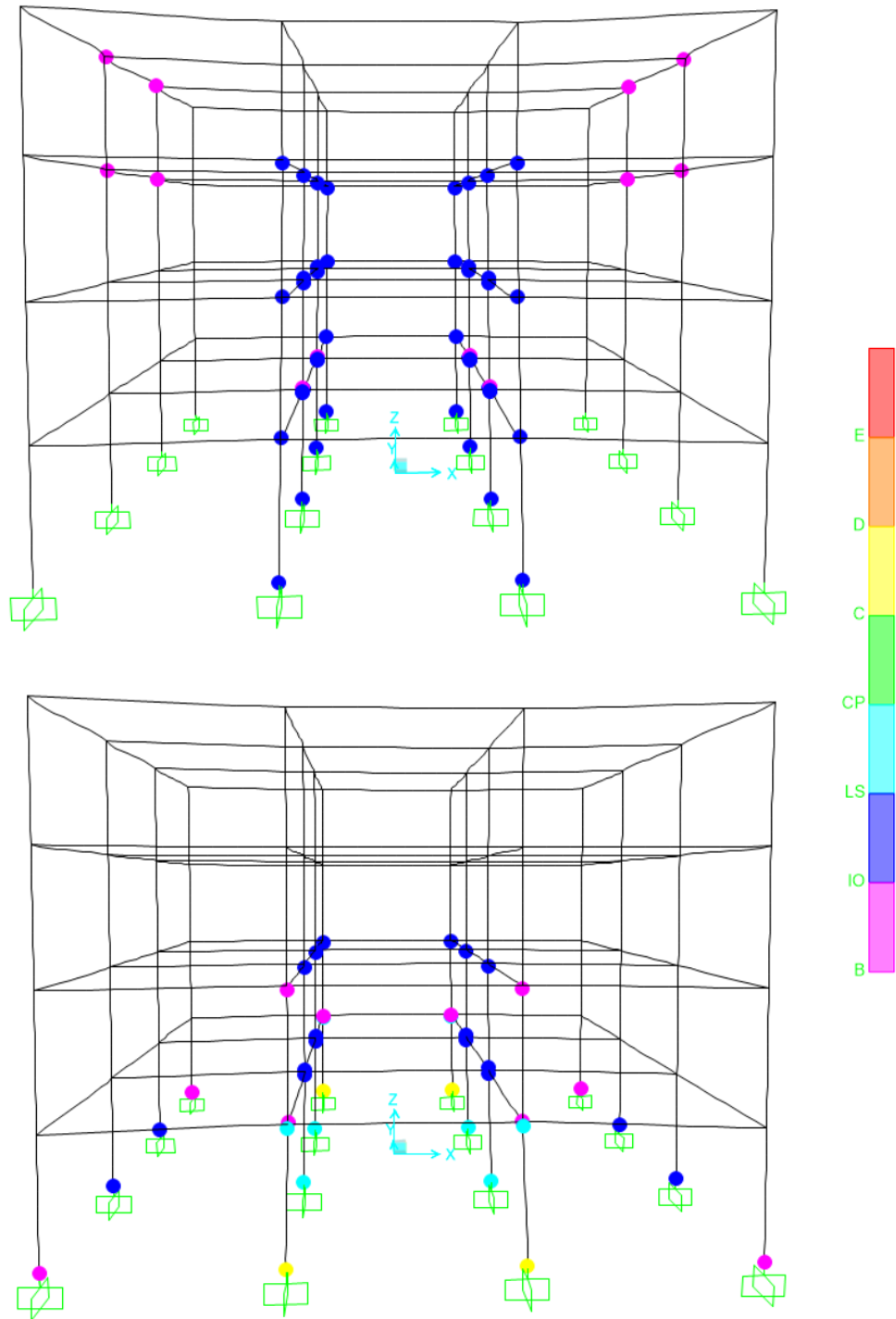


Figure 5.9. Hinge states (BSE-2N) for optimum PBD (top) and FBD (bottom) for Example 3 (+y loading)

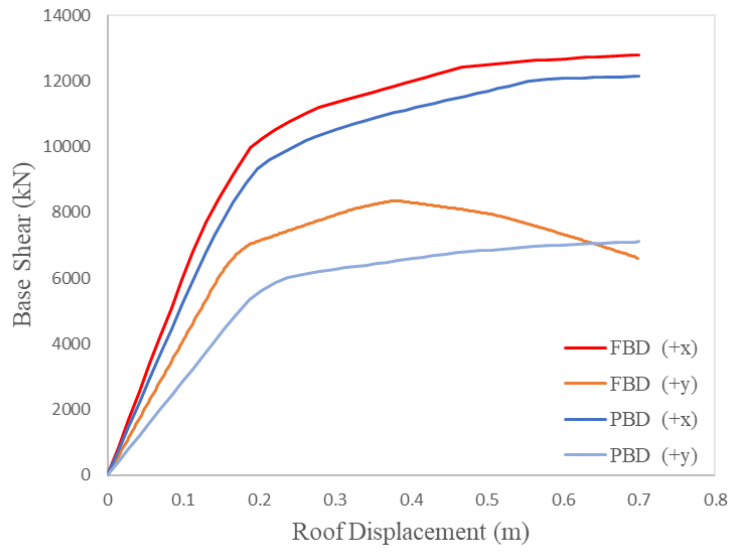


Figure 5.10. Pushover capacity curves of optimum PBD and FBD for Example 3

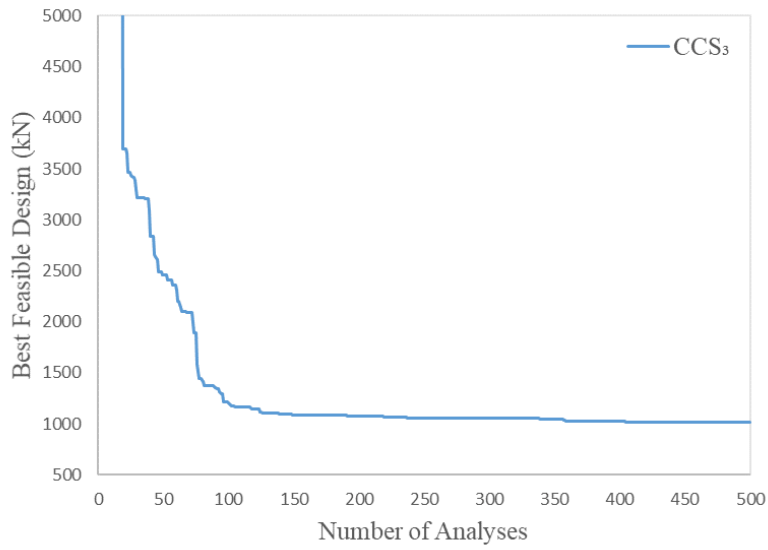


Figure 5.11. Optimization history for Example 3 (PBD)

### 5.3 Summary

The numerical examples presented in this chapter indicate that optimally designed structures according to PBD methodology can be more economical than those optimally designed according to FBD methodology. In general, the PBD methodology leads to lighter design weights up to around 5% in comparison, while the designs are mainly governed by the maximum inter-story drift ratio which is basically defined for limiting damage to non-structural components. It can be concluded that more economical designs could be produced if performance constraints for structural members were considered alone.

Contrary to common expectation that FBD approach is generally conservative, it is shown that the optimum designs of the frames produced according to FBD methodology might fail to satisfy BPOB requirements. On the other hand, the seismic performance of the frames optimally designed according to PBD methodology are ensured inherently as they are subject to performance constraints.

From the optimization point of view, it is demonstrated that the CCS algorithm is also able to handle PBDO problems effectively. Considering the fact that performing numerous nonlinear analyses can take significant amount of time during optimization process, solving PBDO problems by only a few hundreds of analyses is a huge step-forward in terms of practicality.





## CHAPTER 6

### MULTI-OBJECTIVE PERFORMANCE BASED DESIGN OPTIMIZATION

#### 6.1 A Practical Approach for MOPBDO

Metaheuristic optimization techniques are often preferred for solving multi-objective optimization problems. There are basically two reasons behind this preference: (1) they are less susceptible to the continuity or shape of the Pareto front (2) most of the metaheuristic techniques are population-based approaches, and therefore multiple elements of the Pareto optimal set can be found in an iteration. On the other hand, as previously discussed, metaheuristics require a large number of objective function evaluations.

The computational efficiency of the proposed CCS technique in solving single-objective structural optimization problems has been demonstrated in the preceding chapters. A practical approach is adopted in this chapter to employ CCS technique for multi-objective optimization problems, without interfering its search mechanism.

In general, metaheuristics and other optimization techniques that are based on stochastic search moves are run for a predefined number of times to get the best results within the search capability of the algorithms. While the best feasible design obtained during these runs is identified as the final or optimum design, other designs are eliminated. In this study, an archive system is introduced into CCS algorithm to record all these feasible design solutions found until all runs of the optimization process are completed. Then, non-dominated set of solutions are extracted from this archive by using any non-dominated sorting algorithm. Although the non-dominated set of solutions found by this procedure may not always be a good representation of the actual Pareto-optimal set, its implementation is quite simple. In addition, since this is an independent, post-processing procedure, one can define as many objectives as desired and can obtain different trade-off relationships featuring any two of these

objectives (e.g., design weight vs. maximum inter-story drift, design weight vs. a damage index, etc.).

## 6.2 Numerical Examples

For the numerical examples presented in the previous chapter, all the feasible designs located during the performance-based design optimization process are recorded in an archive. The cost-performance trade-off relationship among these designs are established considering design weight and a basic damage index defined as follows:

$$DI = \frac{N_d}{N_T} \quad (6.1)$$

In this equation,  $N_d$  and  $N_T$  represent the number of damaged structural members and the total number of structural members, respectively. A member is considered as damaged if its structural performance is worse than the immediate occupancy level under the BSE-1N earthquake. On the other hand, the BSE-2N earthquake is not considered in the damage index since the examples are designed for collapse prevention building performance level for this hazard level and are assumed irreparable.

For identification of the non-dominated set of solutions among  $N$  feasible designs ( $p$ ) in the archive, the dominance degree approach for non-dominating sort (DDA-NS) (Zhou et al., 2017) is adopted. The algorithm for DDA-NS is as follows:

1. Construct a comparison matrix  $C_{N \times N}$  for each objective function,  $f_k$  of the  $m$ -dimensional multi-objective optimization problem (i.e.,  $k = 1, 2, \dots, m$ ). Each element of this matrix is determined by the following formula:

$$C_{ij}^k = \begin{cases} 0, & \text{if } f_k(p_i) > f_k(p_j) \text{ or } i = j \text{ or } p_i = p_j \\ 1, & \text{if } f_k(p_i) \leq f_k(p_j) \end{cases} \quad (6.2)$$

2. Construct the dominance degree matrix,  $D_{N \times N}$  by summing all comparison matrices as follows:

$$D = \sum_{k=1}^m C^k \quad (6.3)$$

3. Calculate  $D_{max}$ , the row vector containing the maximum value from each column of  $D$ .
4. The designs corresponding to elements of  $D_{max}$  which is less than  $m$  represent the non-dominated set of solutions in the archive.

It is possible via this algorithm to obtain all non-dominated fronts simply by extracting the rows and columns corresponding to non-dominated solutions from the dominance degree matrix ( $D$ ) found in Step 4 and then returning to Step 3, repeatedly until all non-dominated fronts are identified. The first front found by this algorithm will give the closest estimation to the actual Pareto front.

### 6.2.1 Example 1: 28-member planar OMRSF

For the 28-member planar OMRSF, all feasible designs with a design weight less than 200 kN identified throughout the ten runs of the PBDO process are illustrated in Figure 6.1. The non-dominated designs (ND) extracted using DDA-NS algorithm are illustrated in Figure 6.2. These solutions are presented in Table 6.1 as design alternatives for sizing of the frame.

The best feasible design (i.e., minimum weight feasible design) is expected to have 6 damaged structural members (IO to LS) under the design earthquake level (BSE-1N). If this solution is assumed as the global optimum solution for the PBDO problem, the actual pareto front would consist of a maximum of 7 design points (probably less due to symmetrical plan and member grouping), which have a number of damaged members ranging from 0 to 6. It follows that the 4 non-dominated

solutions illustrated in Figure 6.2 may be considered as a good approximation of the actual pareto optimum set since these solutions cover the considered damage index range with even intervals, and with an acceptable distribution of design weights.

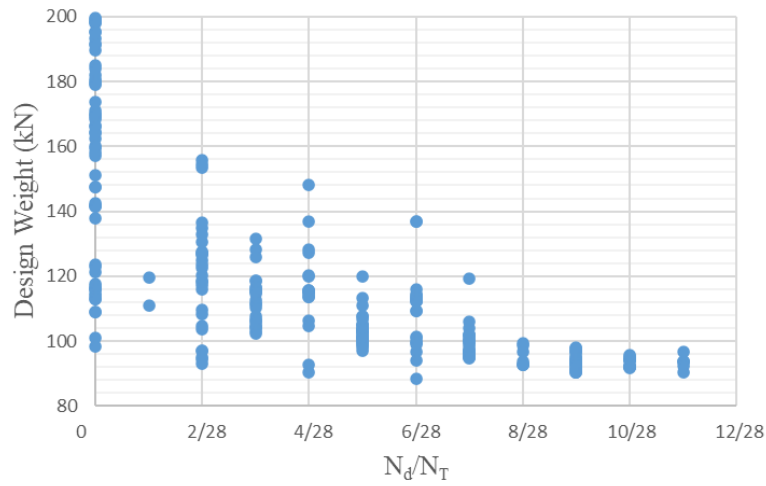


Figure 6.1. Feasible design solutions for Example 1

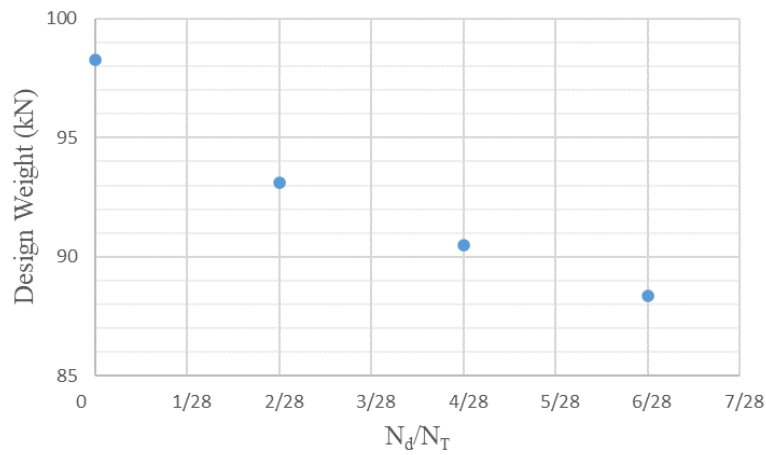


Figure 6.2. Non-dominated design solutions for Example 1

Table 6.1 PBD alternatives for Example 1

<b>Group</b>	<b>ND-1</b>	<b>ND-2</b>	<b>ND-3</b>	<b>ND-4</b>
1	W21x50	W21x50	W21x50	W21x50
2	W18x40	W18x40	W18x40	W18x40
3	W24x94	W24x84	W24x84	W21x83
4	W18x50	W14x43	W12x35	W12x35
5	W24x62	W24x62	W21x57	W21x57
6	W14x43	W12x35	W12x35	W12x26
W (kN)	98.27	93.12	90.48	88.36
$N_d/N_T$	0/28	2/28	4/28	6/28

### 6.2.2 Example 2: 54-member planar OMRSF

For the 54-member planar OMRSF, all feasible designs identified throughout the ten runs of the PBDO process are illustrated in Figure 6.3. The non-dominated designs (ND) extracted using DDA-NS algorithm are illustrated in Figure 6.4. These solutions are presented in Table 6.2 as design alternatives for sizing of the frame.

The best feasible design (i.e., minimum weight feasible design) is expected to have 14 damaged structural members (IO to LS) under the design earthquake level (BSE-1N). If this solution is assumed as the global optimum solution for the PBDO problem, the actual pareto front would consist of a maximum of 15 design points, which have a number of damaged members ranging from 0 to 14. It follows that the 10 non-dominated solutions illustrated in Figure 6.4 may be considered as a fair approximation of the actual pareto optimum set since these solutions cover a significant portion of the considered damage index range (10 out of 15), with an acceptable distribution of design weights.

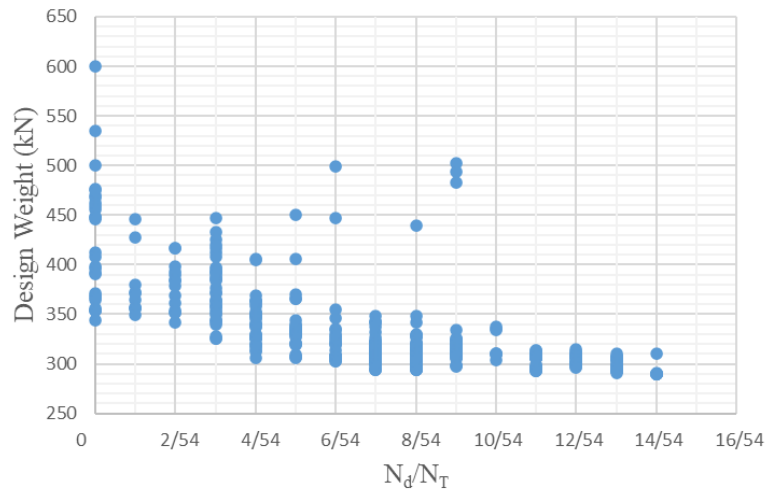


Figure 6.3. Feasible design solutions for Example 2

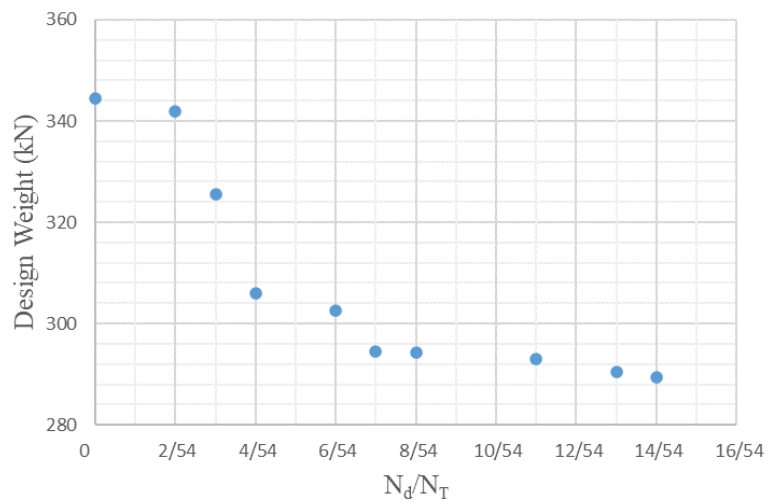


Figure 6.4. Non-dominated design solutions for Example 2

Table 6.2 PBD alternatives for Example 2

Group	ND-1	ND-2	ND-3	ND-4	ND-5	ND-6	ND-7	ND-8	ND-9	ND-10
1	W14x43	W10x30	W14x26	W18x35	W18x35	W16x26	W16x26	W16x26	W16x26	W16x26
2	W10x30	W16x31	W14x26	W14x26	W14x26	W14x26	W14x26	W18x35	W16x26	W16x26
3	W18x35	W18x40	W18x40	W12x26	W12x26	W10x26	W10x26	W10x26	W10x26	W10x26
4	W24x84	W33x130	W30x108	W24x84	W24x84	W24x84	W24x84	W24x84	W30x90	W30x90
5	W24x103	W24x103	W27x102	W27x84	W27x84	W27x84	W27x84	W30x90	W27x84	W27x84
6	W30x90	W24x84	W24x84	W24x84	W24x84	W24x84	W24x84	W24x84	W24x84	W24x84
7	W24x117	W21x62	W16x36	W18x46	W18x46	W16x36	W16x36	W14x34	W16x40	W16x40
8	W44x198	W36x135	W40x149	W36x182	W33x169	W40x167	W40x167	W33x152	W40x149	W40x149
9	W30x108	W33x141	W40x167	W27x102	W30x99	W27x84	W27x84	W30x99	W30x90	W30x90
10	W12x30	W14x34	W14x30	W16x31	W16x31	W16x26	W16x26	W12x26	W16x31	W16x31
11	W36x135	W27x114	W30x108	W30x116	W30x116	W30x108	W30x108	W30x90	W30x90	W30x90
12	W30x90	W27x84	W30x90	W27x84	W30x90	W27x84	W27x84	W30x90	W27x94	W30x90
13	W6x25	W12x35	W6x20	W8x24	W8x24	W10x26	W10x26	W10x26	W12x26	W6x20
14	W30x90	W24x84	W24x84	W27x84	W27x84	W27x84	W24x84	W24x84	W24x84	W24x84
15	W30x90	W24x94	W24x84	W24x84	W24x84	W24x84	W24x84	W24x84	W24x84	W24x84
W (kN)	344.38	341.94	325.59	306.04	302.59	294.46	294.37	293.04	290.40	289.48
$N_d/N_T$	0/54	2/54	3/54	4/54	6/54	7/54	8/54	11/54	13/54	14/54

### 6.2.3 Example 3: 160-member OMRSF

For the 160-member OMRSF, all feasible designs identified 3 throughout the ten runs of the PBDO process are illustrated in Figure 6.5. The non-dominated designs (ND) extracted using DDA-NS algorithm are illustrated in Figure 6.6. These solutions are presented in Table 6.3 as design alternatives for sizing of the frame.

The best feasible design (i.e., minimum weight feasible design) is expected to have 16 damaged structural members (IO to LS) under the design earthquake level (BSE-1N). If this solution is assumed as the global optimum solution for the PBDO problem, the actual pareto front would consist of a maximum of 17 design points (probably less due to symmetrical plan and member grouping), which have a number of damaged members ranging from 0 to 16. It follows that the 7 non-dominated solutions illustrated in Figure 6.6 may be considered as a fair approximation of the actual pareto optimum set since these solutions cover a significant portion of the considered damage index range (7 out of 17), with an acceptable distribution of design weights.

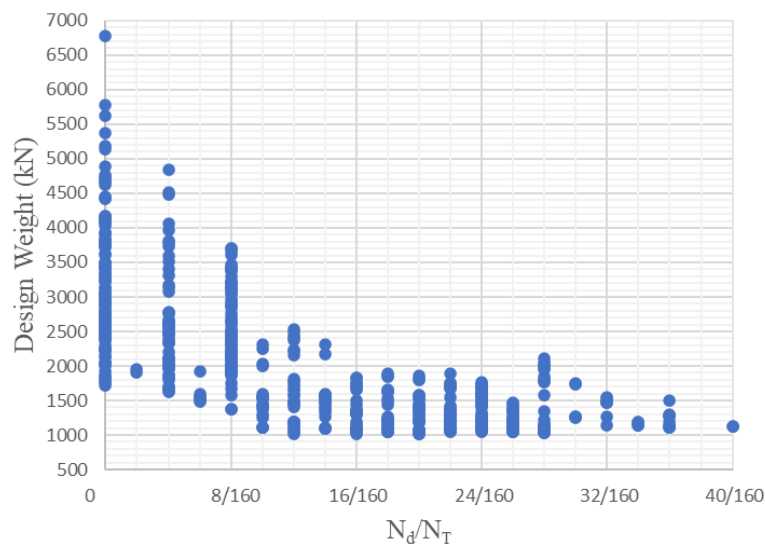


Figure 6.5. Feasible design solutions for Example 3



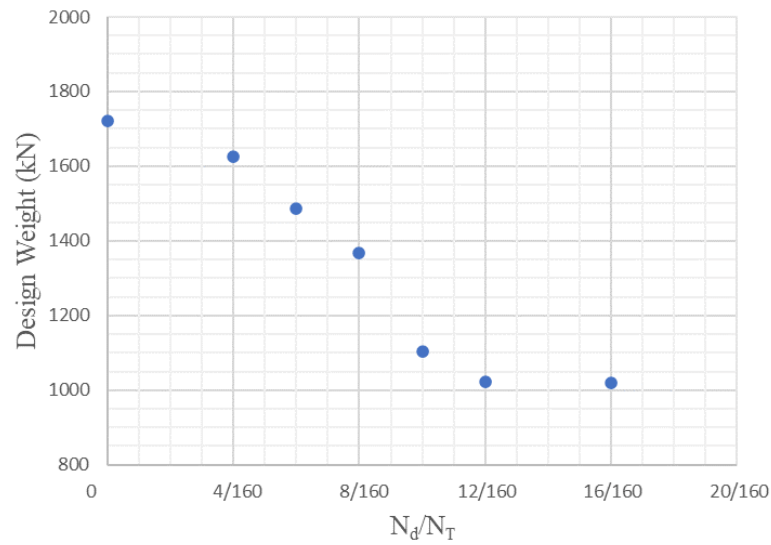


Figure 6.6. Non-dominated design solutions for Example 3

### 6.3 Summary

A practical approach is presented for defining performance-based design alternatives that have varying levels of seismic performance. The approach is based on using a simple damage index formed by the ratio of damaged members to all members, under design earthquake level. In this approach, an archive system which records all feasible designs found during all runs of optimization process is embedded in CCS algorithm. The non-dominated set of solutions is then extracted from this archive by DDA-NS algorithm.

Table 6.3 PBD alternatives for Example 3

Stories	Group	ND-1	ND-2	ND-3	ND-4	ND-5	ND-6	ND-7
1-2	IB	W27x161	W27x102	W27x94	W24x94	W24x84	W27x84	W24x84
	OB	W21x57	W16x50	W30x99	W16x45	W18x46	W12x30	W24x55
	CG <sub>1</sub>	W40x235	W30x261	W33x130	W36x150	W27x84	W30x90	W21x62
	CG <sub>2</sub>	W40x277	W36x280	W36x135	W36x256	W30x116	W33x118	W30x116
	CG <sub>3</sub>	W40x480	W40x328	W33x263	W33x263	W30x211	W40x249	W40x215
	CG <sub>4</sub>	W40x297	W40x324	W36x328	W36x300	W40x328	W36x280	W36x300
	IB	W21x73	W24x84	W24x84	W18x60	W24x62	W21x50	W24x84
	OB	W30x90	W27x102	W30x108	W30x90	W21x68	W18x46	W18x35
3-4	CG <sub>1</sub>	W40x167	W30x261	W30x124	W30x148	W24x76	W30x90	W18x35
	CG <sub>2</sub>	W36x260	W30x261	W33x221	W33x221	W27x114	W24x131	W18x46
	CG <sub>3</sub>	W36x245	W33x263	W27x194	W33x241	W27x217	W33x201	W40x192
	CG <sub>4</sub>	W33x291	W27x258	W27x258	W36x280	W40x221	W36x260	W33x201
	W (kN)	1720.16	1624.77	1485.27	1368.57	1105.17	1022.11	1020.39
	N <sub>d</sub> /N <sub>r</sub>	0/160	4/160	6/160	8/160	10/160	12/160	16/160

## CHAPTER 7

### CONCLUSION

#### 7.1 Summary and Concluding Remarks

In this study, the performance-based design optimization of ordinary moment-resisting steel frames is mainly investigated. The contributions of the study to the field of structural optimization lie in the following three points. First, a novel design-driven optimization technique called Capacity Controlled Search (CCS) is introduced as a robust and time-efficient method for discrete sizing optimization of both conventional force-based design problems and performance-based design problems with/without displacement constraints. Secondly, a comparison of optimally designed ordinary moment-resisting steel frames under PBD and FBD methodologies is provided in terms of cost and seismic performance. Thirdly, a practical approach is proposed to deliver design alternatives under multi-objective optimization framework.

In Chapter 4, the performance of the proposed CCS technique is compared with two metaheuristic search techniques, namely adaptive dimensional search (ADS) and exponential big bang-big crunch (EBB-BC) in terms of convergence characteristics of the algorithms. It is shown that the CCS technique provides computational savings up to ~65-90% in the implemented numerical examples while demonstrating consistent performance. The main advantages of CCS, apart from its simplicity and computational efficiency, can be listed as follows: (1) ability to handle displacement constraints, (2) ability to handle geometric constraints, and (3) being applicable to both FBDO and PBDO problems. In this study, the convergence characteristics of ADS, EBB-BC and CCS techniques are enhanced by the so-called improved upper bound strategy (iUBS), which in fact substantially reduce the computational burden of structural analyses required during the optimization process up to ~45-95% in the

presented numerical examples. In this approach, the penalized weight of a candidate design is calculated first using the weight and the constraints (e.g., geometric constraints) that can be calculated without a need for structural analysis. The candidate design is analyzed and re-evaluated only if its penalized weight is lower than the objective function of the elite design; otherwise, it is rejected automatically without performing a structural analysis since it has no way to be better than the elite design. It is also possible to implement the iUBS dynamically during different phases of structural analyses. For example, after determining local response constraints (e.g., stresses, deflections, etc.) first, the penalized weight of a candidate design is updated and checked whether it is still able to improve the elite design. If it is not, later phases of structural analyses like determining story drift ratios or hinge states (if it is PBDO) can be skipped to avoid unnecessary computations.

In Chapter 5, it is shown that the structures that are designed optimally according to PBD methodology are lighter than those designed optimally according to conventional FBD methodology up to around 5%. It should also be noted that a specified level of seismic performance is ensured inherently by the PBD. The results indicate that the performance-based design methodology may offer some advantages in terms of economy and safety with respect to conventional force-based design.

In Chapter 6, an archive system is employed, in which all feasible design solutions identified during PBDO runs are recorded for determining performance-based design alternatives. Then, the non-dominated designs are extracted from this archive by using DDA-NS algorithm as a post-process. The proposed approach, rather than finding the true pareto front, aims to determine the hierarchy among all recorded designs and present a set of design alternatives for decision makers. Since it is a post-processing approach, it does not interfere the search process or slow down the convergence rate of the optimization technique. The main advantage of this approach is its scalability such that one can define as many objectives (design weight, inter-story drift or multiple damage indices, etc.) as desired based on engineering preferences and extract non-dominated solutions from the archive accordingly.

Following remarks can be made based on this study:

- CCS is a simple, robust, and fast design-driven optimization algorithm that can be applied to both FBDO and PBDO problems with/without displacement constraints.
- CCS is able to produce cost-efficient, code-compliant designs by requiring only in scale of hundreds of structural analyses or response calculations, which is much less than that is required for metaheuristics.
- iUBS is a simple and efficient procedure to reduce number of analyses required during optimization process and can be also applied in conjunction with many other optimization techniques with elitism approach.
- Optimally designed steel moment frames under PBD methodology are inherently safer and can be more economical than those optimally designed by conventional FBD approach.
- Despite the common expectation that FBD approach is generally conservative, optimum FBD of steel moment frame examples demonstrated inadequate seismic performance when evaluated in accordance with ASCE 41-13.
- Optimum PBD of steel moment frames is mainly governed by inter-story drift ratio constraints, which is in fact defined for limiting damage to non-structural components. More economical designs can be produced by PBD approach if the damage to structural components is considered alone.

## **7.2 Recommendations for Future Research**

Over the last two decades, there is a growing interest in PBD, especially under structural optimization framework. Nevertheless, the relevant studies in the field are still scarce, and a shift from conventional FBD to PBD is highly dependent on the research efforts. The findings in this study suggest that ordinary moment-resisting steel frames can be designed more economically and safely by PBDO approach than by FBDO approach. It is worthwhile to scrutinize economical aspects of PBDO on

different type of structures, such as braced steel frames and reinforced concrete structures. Finally, it is recommended that the performance of the existing design-driven optimization techniques in conjunction with PBDO should be investigated. In this regard, developing simple and efficient optimization techniques will surely contribute to a widespread use of optimization tools in structural engineering design applications.

## REFERENCES

- Ahrari, A., & Atai, A. A. (2013). Fully stressed design evolution strategy for shape and size optimization of truss structures. *Computers and Structures*, *123*, 58–67. <https://doi.org/10.1016/j.compstruc.2013.04.013>
- Ahrari, A., & Deb, K. (2016). An improved fully stressed design evolution strategy for layout optimization of truss structures. *Computers and Structures*, *164*, 127–144. <https://doi.org/10.1016/j.compstruc.2015.11.009>
- American Society of Civil Engineers. (2007). *ASCE/SEI 41-06: Seismic rehabilitation of existing buildings*.
- American Society of Civil Engineers. (2014). *ASCE/SEI 41-13: Seismic evaluation and retrofit of existing buildings*.
- American Society of Civil Engineers. (2017). *ASCE/SEI 41-17: Seismic evaluation and retrofit of existing buildings*.
- Applied Technology Council. (1996). *ATC-40: Seismic evaluation and retrofit of existing concrete buildings*.
- Burchart-Korol, D. (2013). Life cycle assessment of steel production in Poland: A case study. *Journal of Cleaner Production*, *54*, 235–243. <https://doi.org/10.1016/j.jclepro.2013.04.031>
- Chan, C. M. (2001). Optimal lateral stiffness design of tall buildings of mixed steel and concrete construction. *Structural Design of Tall Buildings*, *10*(3), 155–177. <https://doi.org/10.1002/tal.170>
- Cheng, M. Y., Prayogo, D., Wu, Y. W., & Lukito, M. M. (2016). A Hybrid Harmony Search algorithm for discrete sizing optimization of truss structure. *Automation in Construction*, *69*, 21–33. <https://doi.org/10.1016/j.autcon.2016.05.023>
- Chopra, A. K., & Goel, R. K. (2002). A modal pushover analysis procedure for

- estimating seismic demands for buildings. *Earthquake Engineering and Structural Dynamics*, 31(3), 561–582. <https://doi.org/10.1002/eqe.144>
- Chopra, A. K., Goel, R. K., & Chintanapakdee, C. (2004). Evaluation of a modified MPA procedure assuming higher modes as elastic to estimate seismic demands. *Earthquake Spectra*, 20(3), 757–778. <https://doi.org/10.1193/1.1775237>
- Degertekin, S. O., Tutar, H., & Lamberti, L. (2020). School-based optimization for performance-based optimum seismic design of steel frames. *Engineering with Computers*, 0123456789. <https://doi.org/10.1007/s00366-020-00993-1>
- Di Schino, A. (2019). Environmental Impact of Steel Industry. *Handbook of Environmental Materials Management*, 2463–2483. [https://doi.org/10.1007/978-3-319-73645-7\\_101](https://doi.org/10.1007/978-3-319-73645-7_101)
- Elnashai, A. S. (2001). Advanced inelastic static (pushover) analysis for earthquake applications. *Structural Engineering and Mechanics*, 12(1), 51–69. <https://doi.org/10.12989/sem.2001.12.1.051>
- Elvin, A., Walls, R., & Cromberge, D. (2009). Optimising structures using the principle of virtual work. *Journal of the South African Institution of Civil Engineering*, 51(2), 11–19.
- Eom, T. S., Park, H. G., & Lee, C. H. (2013). Simplified method for estimation of beam plastic rotation demand in special moment-resisting steel-frame structures. *Journal of Structural Engineering (United States)*, 139(11), 1906–1916. [https://doi.org/10.1061/\(ASCE\)ST.1943-541X.0000768](https://doi.org/10.1061/(ASCE)ST.1943-541X.0000768)
- Federal Emergency Management Agency. (1997). *FEMA-273: NEHRP Guidelines for the seismic rehabilitation of buildings*.
- Federal Emergency Management Agency. (2000). *FEMA-356: Prestandard and commentary for the seismic rehabilitation of buildings*.
- Flager, F., Soremekun, G., Adya, A., Shea, K., Haymaker, J., & Fischer, M. (2011). Fully Constrained Design: a Scalable Method for Discrete Member Sizing



Optimization of Steel Frame Structures. *CIFE Technical Report #TR201*, September, 1–34.

Fragiadakis, M., Lagaros, N. D., & Papadrakakis, M. (2006). Performance-based multiobjective optimum design of steel structures considering life-cycle cost. *Structural and Multidisciplinary Optimization*, 32(1), 1–11. <https://doi.org/10.1007/s00158-006-0009-y>

Gholizadeh, S. (2015). Performance-based optimum seismic design of steel structures by a modified firefly algorithm and a new neural network. *Advances in Engineering Software*, 81(C), 50–65. <https://doi.org/10.1016/j.advengsoft.2014.11.003>

Gholizadeh, S., & Baghchevan, A. (2017). Multi-objective seismic design optimization of steel frames by a chaotic meta-heuristic algorithm. *Engineering with Computers*, 33(4), 1045–1060. <https://doi.org/10.1007/s00366-017-0515-0>

Gholizadeh, S., & Fattahi, F. (2019). Multi-objective design optimization of steel moment frames considering seismic collapse safety. *Engineering with Computers*, 0123456789. <https://doi.org/10.1007/s00366-019-00886-y>

Gholizadeh, S., Kamyab, R., & Dadashi, H. (2012). Performance-based design optimization of steel moment frames. *International Journal of Optimization in Civil Engineering*, 3(2), 327–343.

Gholizadeh, S., & Milany, A. (2016). Optimal performance-based design of steel frames using advanced metaheuristics. *Asian Journal of Civil Engineering*, 17(5), 607–623.

Gholizadeh, S., & Moghadas, R. (2014). Performance-Based Optimum Design of Steel Frames by an Improved Quantum Particle Swarm Optimization. *Advances in Structural Engineering*, 17(2), 143–156. <https://doi.org/10.1260/1369-4332.17.2.143>

- Ghosh, S., Datta, D., & Katakdhond, A. A. (2011). Estimation of the Park-Ang damage index for planar multi-storey frames using equivalent single-degree systems. *Engineering Structures*, 33(9), 2509–2524.  
<https://doi.org/10.1016/j.engstruct.2011.04.023>
- Gupta, B., & Kunnath, S. K. (2000). Adaptive spectra-based pushover procedure for seismic evaluation of structures. In *Earthquake Spectra* (Vol. 16, Issue 2, pp. 367–391). <https://doi.org/10.1193/1.1586117>
- Hasançebi, O., Bahçecioğlu, T., Kurç, Ö., & Saka, M. P. (2011). Optimum design of high-rise steel buildings using an evolution strategy integrated parallel algorithm. *Computers and Structures*, 89(21–22), 2037–2051.  
<https://doi.org/10.1016/j.compstruc.2011.05.019>
- Hasançebi, O., Çarbaş, S., Doğan, E., Erdal, F., & Saka, M. P. (2009). Performance evaluation of metaheuristic search techniques in the optimum design of real size pin jointed structures. *Computers and Structures*, 87(5–6), 284–302.  
<https://doi.org/10.1016/j.compstruc.2009.01.002>
- Hasançebi, O., Çarbaş, S., Doğan, E., Erdal, F., & Saka, M. P. (2010). Comparison of non-deterministic search techniques in the optimum design of real size steel frames. *Computers and Structures*, 88(17–18), 1033–1048.  
<https://doi.org/10.1016/j.compstruc.2010.06.006>
- Hasançebi, O., & Kazemzadeh Azad, S. (2012). An exponential big bang-big crunch algorithm for discrete design optimization of steel frames. *Computers and Structures*, 110–111, 167–179.  
<https://doi.org/10.1016/j.compstruc.2012.07.014>
- Hasançebi, O., & Azad, S. K. (2015). Adaptive dimensional search: A new metaheuristic algorithm for discrete truss sizing optimization. *Computers and Structures*, 154, 1–16. <https://doi.org/10.1016/j.compstruc.2015.03.014>
- Hasançebi, O., & Kazemzadeh Azad, S. (2019). Discrete sizing of steel frames using

- adaptive dimensional search algorithm. *Periodica Polytechnica Civil Engineering*, 63(4), 1062–1079. <https://doi.org/10.3311/PPci.14746>
- Hernández-Montes, E., Kwon, O. S., & Aschheim, M. A. (2004). An energy-based formulation for first- and multiple-mode nonlinear static (Pushover) analyses. *Journal of Earthquake Engineering*, 8(1), 69–88. <https://doi.org/10.1080/13632460409350481>
- Hill, M. P., & Rossetto, T. (2008). Do Existing Damage Scales Meet The Needs Of Seismic Loss Estimation? *The 14th World Conference on Earthquake Engineering*, 6(2), 335–365. <http://www.springerlink.com/content/7125261h28t31871/>
- Kaatsız, K., & Sucuoglu, H. (2014). Generalized force vectors for multi-mode pushover analysis of torsionally coupled systems. *Earthquake Engineering and Structural Dynamics*, 43, 2015–2033. <https://doi.org/10.1002/eqe>
- Kalkan, E., & Kunnath, S. K. (2006). Adaptive modal combination procedure for nonlinear static analysis of building structures. *Journal of Structural Engineering*, 132(11), 1721–1731. [https://doi.org/10.1061/\(ASCE\)0733-9445\(2006\)132:11\(1721\)](https://doi.org/10.1061/(ASCE)0733-9445(2006)132:11(1721))
- Karami Mohammadi, R., & Ghasemof, A. (2015). Performance-based design optimization using uniform deformation theory: A comparison study. *Latin American Journal of Solids and Structures*, 12(1), 18–36. <https://doi.org/10.1590/1679-78251207>
- Kaveh, A., Bakhshpoori, T., & Afshari, E. (2014). An efficient hybrid Particle Swarm and Swallow Swarm Optimization algorithm. *Computers and Structures*, 143, 40–59. <https://doi.org/10.1016/j.compstruc.2014.07.012>
- Kaveh, A., Farahmand Azar, B., Hadidi, A., Rezazadeh Sorochi, F., & Talatahari, S. (2010). Performance-based seismic design of steel frames using ant colony optimization. *Journal of Constructional Steel Research*, 66(4), 566–574. <https://doi.org/10.1016/j.jcsr.2009.11.006>

- Kaveh, A, Gholipour, Y., & Rahami, H. (2008). Optimal design of transmission towers using genetic algorithm and neural networks. *International Journal of Space Structures*, 23(1), 1–19. <https://doi.org/10.1260/026635108785342073>
- Kaveh, A, & Ilchi Ghazaan, M. (2018). A new hybrid meta-heuristic algorithm for optimal design of large-scale dome structures. *Engineering Optimization*, 50(2), 235–252. <https://doi.org/10.1080/0305215X.2017.1313250>
- Kaveh, A, & Mahdavi, V. R. (2015). A hybrid CBO-PSO algorithm for optimal design of truss structures with dynamic constraints. *Applied Soft Computing Journal*, 34, 260–273. <https://doi.org/10.1016/j.asoc.2015.05.010>
- Kaveh, A, & Nasrollahi, A. (2014). Performance-based seismic design of steel frames utilizing charged system search optimization. *Applied Soft Computing Journal*, 22, 213–221. <https://doi.org/10.1016/j.asoc.2014.05.012>
- Kaveh, A, & Talatahari, S. (2012). A hybrid CSS and PSO algorithm for optimal design of structures. *Structural Engineering and Mechanics*, 42(6), 783–797. <https://doi.org/10.12989/sem.2012.42.6.783>
- Kaveh, Ali, Laknejadi, K., & Alinejad, B. (2012). Performance-based multi-objective optimization of large steel structures. *Acta Mechanica*, 223(2), 355–369. <https://doi.org/10.1007/s00707-011-0564-1>
- Kazemzadeh Azad, S. (2014). *Computationally enhanced techniques for practical optimum design of steel structures (PhD Thesis)*. Middle East Technical University.
- Kazemzadeh Azad, S. (2017). Enhanced hybrid metaheuristic algorithms for optimal sizing of steel truss structures with numerous discrete variables. *Structural and Multidisciplinary Optimization*, 55(6), 2159–2180. <https://doi.org/10.1007/s00158-016-1634-8>
- Kazemzadeh Azad, S., & Hasançebi, O. (2015). Computationally efficient discrete sizing of steel frames via guided stochastic search heuristic. *Computers and*

*Structures*, 156, 12–28. <https://doi.org/10.1016/j.compstruc.2015.04.009>

Kazemzadeh Azad, S., Hasançebi, O., & Kazemzadeh Azad, S. (2013). Upper bound strategy for metaheuristic based design optimization of steel frames. *Advances in Engineering Software*, 57, 19–32.

<https://doi.org/10.1016/j.advengsoft.2012.11.016>

Kazemzadeh Azad, S., Hasançebi, O., & Saka, M. P. (2014). Guided stochastic search technique for discrete sizing optimization of steel trusses: A design-driven heuristic approach. *Computers and Structures*, 134, 62–74.

<https://doi.org/10.1016/j.compstruc.2014.01.005>

Kreslin, M., & Fajfar, P. (2012). The extended N2 method considering higher mode effects in both plan and elevation. *Bulletin of Earthquake Engineering*, 10(2), 695–715. <https://doi.org/10.1007/s10518-011-9319-6>

Li, G., Jiang, Y., & Yang, D. (2012). Modified-modal-pushover-based seismic optimum design for steel structures considering life-cycle cost. *Structural and Multidisciplinary Optimization*, 45(6), 861–874.

<https://doi.org/10.1007/s00158-011-0740-x>

Liang, J. C., Li, L. J., & He, J. N. (2015). Performance-based multi-objective optimization design for steel structures with intelligence algorithms. *International Journal of Optimization in Civil Engineering*, 5(1), 79–101.

<http://ijoc.e.iust.ac.ir/article-1-200-en.pdf>

Liu, M., Burns, S. A., & Wen, Y. K. (2005). Multiobjective optimization for performance-based seismic design of steel moment frame structures. *Earthquake Engineering and Structural Dynamics*, 34(3), 289–306.

<https://doi.org/10.1002/eqe.426>

Mokarram, V., & Banan, M. R. (2018). An improved multi-objective optimization approach for performance-based design of structures using nonlinear time-history analyses. *Applied Soft Computing Journal*, 73, 647–665.

<https://doi.org/10.1016/j.asoc.2018.08.048>

- Moynihan, M. C., & Allwood, J. M. (2012). The flow of steel into the construction sector. *Resources, Conservation and Recycling*, 68, 88–95. <https://doi.org/10.1016/j.resconrec.2012.08.009>
- Olmez, G. M., Dilek, F. B., Karanfil, T., & Yetis, U. (2016). The environmental impacts of iron and steel industry: A life cycle assessment study. *Journal of Cleaner Production*, 130, 195–201. <https://doi.org/10.1016/j.jclepro.2015.09.139>
- Papadrakakis, M., Lagaros, N. D., & Fragakis, Y. (2003). Parallel computational strategies for structural optimization. *International Journal for Numerical Methods in Engineering*, 58(9), 1347–1380. <https://doi.org/10.1002/nme.821>
- Papadrakakis, M., Lagaros, N. D., & Tsompanakis, Y. (1998). Structural optimization using evolution strategies and neural networks. *Computer Methods in Applied Mechanics and Engineering*, 156(1–4), 309–333. [https://doi.org/10.1016/S0045-7825\(97\)00215-6](https://doi.org/10.1016/S0045-7825(97)00215-6)
- Park, H. S., & Park, C. L. (1997). Drift control of high-rise buildings with unit load method. *Structural Design of Tall Buildings*, 6(1), 23–35. [https://doi.org/10.1002/\(SICI\)1099-1794\(199703\)6:1<23::AID-TAL80>3.0.CO;2-1](https://doi.org/10.1002/(SICI)1099-1794(199703)6:1<23::AID-TAL80>3.0.CO;2-1)
- Patnaik, S. N., Gendy, A. S., Berke, L., & Hopkins, D. A. (1998). Modified fully utilized design (MFUD) method for stress and displacement constraints. *International Journal for Numerical Methods in Engineering*, 41(7), 1171–1194. [https://doi.org/10.1002/\(SICI\)1097-0207\(19980415\)41:7<1171::AID-NME296>3.0.CO;2-O](https://doi.org/10.1002/(SICI)1097-0207(19980415)41:7<1171::AID-NME296>3.0.CO;2-O)
- Priestley, M. J. N., Calvi, G. M., & Kowalsky, M. J. (2007). *Displacement-based seismic design of structures*. IUSS Press.
- Reyes, J. C., & Chopra, A. K. (2011). Three-dimensional modal pushover analysis of buildings subjected to two components of ground motion, including its evaluation for tall buildings Juan. *Earthquake Engineering and Structural*

*Dynamics*, 40, 789–806. <https://doi.org/10.1002/eqe>

Saka, M. P., Hasańcebi, O., & Geem, Z. W. (2016). Metaheuristics in structural optimization and discussions on harmony search algorithm. *Swarm and Evolutionary Computation*, 28, 88–97.

<https://doi.org/10.1016/j.swevo.2016.01.005>

Sarma, K. C., & Adeli, H. (2001). Bilevel parallel genetic algorithms for optimization of large steel structures. *Computer-Aided Civil and Infrastructure Engineering*, 16(5), 295–304. <https://doi.org/10.1111/0885-9507.00234>

Soleimani, S., Aziminejad, A., & Moghadam, A. S. (2017). Extending the concept of energy-based pushover analysis to assess seismic demands of asymmetric-plan buildings. *Soil Dynamics and Earthquake Engineering*, 93(November 2016), 29–41. <https://doi.org/10.1016/j.soildyn.2016.11.014>

Structural Engineers Association of California (SEAOC). (1995). *Vision 2000: Performance based seismic engineering of buildings*.

Sucuoglu, H., & Günay, M. S. (2011). Generalized force vectors for multi-mode pushover analysis. *Earthquake Engineering and Structural Dynamics*, 40, 55–74. <https://doi.org/10.1002/eqe>

Ting, T. O., Yang, X. S., Cheng, S., & Huang, K. (2015). Hybrid metaheuristic algorithms: Past, present, and future. *Studies in Computational Intelligence*, 585(January), 71–83. [https://doi.org/10.1007/978-3-319-13826-8\\_4](https://doi.org/10.1007/978-3-319-13826-8_4)

Tongpool, R., Jirajariyavech, A., Yuvaniyama, C., & Mungcharoen, T. (2010). Analysis of steel production in Thailand: Environmental impacts and solutions. *Energy*, 35(10), 4192–4200. <https://doi.org/10.1016/j.energy.2010.07.003>

Walls, R., & Elvin, A. (2010). Optimizing structures subject to multiple deflection constraints and load cases using the principle of virtual work. *Journal of Structural Engineering*, 136(11), 1444–1452.

[https://doi.org/10.1061/\(ASCE\)ST.1943-541X.0000246](https://doi.org/10.1061/(ASCE)ST.1943-541X.0000246)

- Wang, T., Müller, D. B., & Graedel, T. E. (2007). Forging the anthropogenic iron cycle. *Environmental Science and Technology*, *41*(14), 5120–5129.  
<https://doi.org/10.1021/es062761t>
- Wang, X., Zhang, Q., Qin, X., & Sun, Y. (2020). An efficient discrete optimization algorithm for performance-based design optimization of steel frames. *Advances in Structural Engineering*, *23*(3), 411–423.  
<https://doi.org/10.1177/1369433219872440>
- Wen, Y. K., & Kang, Y. J. (2001). Minimum Building Life-Cycle Cost Design Criteria. II: Applications. *Journal of Structural Engineering (United States)*, *127*(3), 330–337.
- Zhou, Y., Chen, Z., & Zhang, J. (2017). Ranking vectors by means of the dominance degree matrix. *IEEE Transactions on Evolutionary Computation*, *21*(1), 34–51.  
<https://doi.org/10.1109/TEVC.2016.2567648>
- Zou, X. K., Chan, C. M., Li, G., & Wang, Q. (2007). Multiobjective optimization for performance-based design of reinforced concrete frames. *Journal of Structural Engineering*, *133*(10), 1462–1474. [https://doi.org/10.1061/\(ASCE\)0733-9445\(2007\)133:10\(1462\)](https://doi.org/10.1061/(ASCE)0733-9445(2007)133:10(1462))



## CURRICULUM VITAE

### PERSONAL INFORMATION

Surname, Name: Eser, Hasan  
Nationality: Turkish (TC)  
Date and Place of Birth: 1988, Ankara  
email: heser@metu.edu.tr

### EDUCATION

<b>Degree</b>	<b>Institution</b>	<b>Year of Graduation</b>
MS	METU Civil Engineering	2014
BS	METU Civil Engineering	2011
High School	Ankara Atatürk High School	2006

### WORK EXPERIENCE

<b>Year</b>	<b>Place</b>	<b>Enrollment</b>
2011-2020	METU Dept. of Civil Eng.	Research Assistant

### FOREIGN LANGUAGES

Fluent English, Basic Japanese